Numer Algor
DOI 10.1007/s11075-012-9677-4

ORIGINAL PAPER

A new triangular spectral element method I: implementation and analysis on a triangle

Michael Daniel Samson · Huiyuan Li · Li-Lian Wang

Received: 11 April 2012 / Accepted: 23 November 2012

Abstract This paper serves as our first effort to develop a new triangular spectral element method (TSEM) on unstructured meshes, using the rectangle–triangle mapping proposed in the conference note (Li et al. 2011). Here, we provide some new insights into the originality and distinctive features of the mapping, and show that this transform only induces a logarithmic singularity, which allows us to devise a fast, stable and accurate numerical algorithm for its removal. Consequently, any triangular element can be treated as efficiently as a quadrilateral element, which affords a great flexibility in handling complex computational domains. Benefited from the fact that the image of the mapping includes the polynomial space as a subset, we are able to obtain optimal L^2- and H^1-estimates of approximation by the proposed basis functions on triangle. The implementation details and some numerical examples are provided to validate the efficiency and accuracy of the proposed method. All these will pave the way for developing an unstructured TSEM based on, e.g., the hybridizable discontinuous Galerkin formulation.

Keywords Rectangle–triangle mapping · Consistency condition · Triangular spectral elements · Spectral accuracy

The research of Michael Daniel Samson and Li-Lian Wang is partially supported by Singapore AcRF Tier 1 Grant RG58/08.

The work of Huiyuan Li was supported by National Natural Science Foundation of China (NSFC) Grants 10601056 and 10971212.

M. D. Samson · L.-L. Wang (✉)
Division of Mathematical Sciences, School of Physical and Mathematical Sciences, Nanyang Technological University, Singapore 637371, Singapore
e-mail: lilian@ntu.edu.sg

H. Li
Institute of Software, Chinese Academy of Sciences, Beijing 100190, China

Published online: 27 December 2012

Mathematics Subject Classifications (2010) 65N35 · 65N22 · 65F05 · 35J05

1 Introduction

The spectral element method (SEM), originated from Patera [31], integrates the unparalleled accuracy of spectral methods with the geometric flexibility of finite elements, and also enjoys a high-level parallel computer architecture. Nowadays, it has become a pervasive numerical technique for simulating challenging problems in complex domains [4, 10]. While the classical SEM on quadrilateral/hexahedral elements (QSEM) exhibits the advantages of using tensorial basis functions and naturally diagonal mass matrices, the need for high-order methods on unstructured meshes with robust adaptivity spawns the development of triangular/tetrahedral spectral elements. In general, research efforts along this line fall into three trends: (1) nodal TSEM based on high-order polynomial interpolation on special interpolation points [6, 20, 36]; (2) modal TSEM based on the Koornwinder–Dubiner (KD) polynomials [11, 22, 24]; and (3) approximation by non-polynomial functions [5, 26, 34].

The question of how to construct "good" interpolation points for stable high-order polynomial interpolation on the triangle is still quite subtle and somehow open. The strict analogy of the Gauss–Lobatto integration rule on quadrilaterals/hexahedra does not exist on triangles [19], though a "relaxed" rule can be constructed in the sense of [40]. We refer to [30] for an up-to-date review and a very dedicated comparative study of various criteria for constructing workable interpolation points on triangle. In general, such points have low degree of precision (i.e., exactness for integration of polynomials), and this motivates the use of a different set of points for integration (see [29]), which are mapped from the Gauss points on the reference square via the Duffy's transform [12].

The development of TSEM using KD polynomials as modal basis functions, generated by the rectangle–triangle mapping (i.e., the Duffy's transform), can be best attested to by the monograph [22] and the spectral-element package *Nektar++* (http://www.nektar.info/). The analysis of this approach can be found in e.g., [7, 17, 25, 32]. The KD basis is intrinsically built on a warped tensor product, which is mimic to the spherical harmonic functions. One gain from lacking the full tensorial structure is the use of polynomials of total degree not more than a cutoff number N that halves the degrees of freedom involving a usual tensor-based approximation. One argument against the transform is that the mapped interpolation points are unfavorably clustered near the singular vertex of the triangle. The situation is even severer in the three-dimensional case, where one face of the reference cube is collapsed into a vertex of the reference tetrahedron. We remark that a full tensorial rational approximation on triangles was proposed in [34] for elliptic problems, and extended to the Stokes problem in [5], while this approach was still based on the Duffy's transform. It also requires to modify the tensorial polynomial basis to meet the underlying consistency conditions (analogous to "pole conditions" in polar/spherical coordinates) induced by the singularity of the transform. It is worthwhile to point out that the use of the Gauss–Radau points, which exclude the endpoint corresponding to the singular vertex, mitigates some numerical difficulties in dealing with the singularity.

Our mind-set is therefore driven by searching for a method based on a different rectangle–triangle mapping that can lead to favorable distributions of interpolation/quadrature points on the triangle without loss of accuracy and efficiency of implementation. With this in mind, we introduced in the conference note [27] a new mapping that pulls one side (at the middle point) of the triangle to two sides of the rectangle (cf. Fig. 1a), and results in relatively desirable distributions of the mapped LGL points (cf. Fig. 1c vs. d). Moreover, this mapping is one–to–one.

The purposes of this paper are threefold: (1) have some new insights into this mapping; (2) demonstrate that the singularity of the mapping is of logarithmic type, which can be fully removed; and (3) derive optimal error estimates for approximation by the associated basis functions. This work will pave the way for developing a new TSEM on unstructured meshes, which will be explored in the second part. It also brings about an important viewpoint that any triangular element can be mapped to the reference square via a composite of the rectangle–triangle mapping and an affine mapping, and with the successful removal of the singularity, the triangular element can be treated as efficiently as a quadrilateral element. One implication is that this allows a mixture of triangular and quadrilateral elements, so one can handle more complex domains with more regular computational meshes, e.g., by tiling the triangular elements along the boundary of the domain. More importantly, for general unstructured triangular meshes, we can formulate the underlying variational problems using the recently enhanced hybridizable discontinuous Galerkin methods [9, 23, 28]. We expect that the QSEM will enjoy a minimal communication between elements, and a minimum number of globally coupled degrees of freedom, and allow for implementing a large degree of nonconformity across elements (e.g., the hanging nodes and mortaring techniques). We leave this development to the second part after this work.

The rest of this paper is organized as follows. In Section 2, we present some new insights of the rectangle–triangle mapping. In Section 3, we introduce the basis functions and the efficient algorithm for computing the stiffness and mass matrices with an emphasis on how to remove the singularity of the rectangle–triangle transform. We derive some optimal approximation results in Section 4, followed by numerical results on a triangle in Section 5.

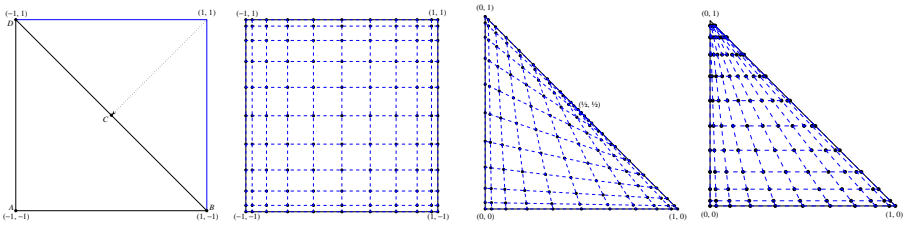

Fig. 1 **a** $\triangle \leftrightarrow \square$ mapping; **b** tensorial Legendre–Gauss–Lobatto (LGL) points on $\square$; **c** mapped LGL grids on $\triangle$; **d** mapped LGL grids on $\triangle$ using the Duffy's transform

2 The rectangle–triangle mapping

We collect in this section some properties of the rectangle–triangle mapping introduced in [27], and provide some insightful perspectives on this transform.

2.1 The rectangle–triangle mapping

Throughout the paper, we denote by

$$\triangle := \big\{(x, y) : 0 < x, y, x+y < 1\big\} \subset \mathbb{R}^2, \quad \square := \big\{(\xi, \eta) : -1 < \xi, \eta < 1\big\} \subset \mathbb{R}^2,$$

the *reference triangle* and the *reference square*, respectively. Here, we denote by $\mathbb{R}$ the set of all real numbers. The rectangle–triangle transform (cf. [27]) $T : \square \to \triangle$, takes the form

$$x = \frac{1}{8}(1+\xi)(3-\eta), \quad y = \frac{1}{8}(3-\xi)(1+\eta), \quad \forall\ (\xi, \eta) \in \square, \tag{2.1}$$

with the inversion $T^{-1} : \triangle \to \square$:

$$\begin{cases} \xi = 1 + (x-y) - \sqrt{(x-y)^2 + 4(1-x-y)}, \\ \eta = 1 - (x-y) - \sqrt{(x-y)^2 + 4(1-x-y)}, \end{cases} \tag{2.2}$$

for any $(x, y) \in \triangle$. It maps the vertices $(-1, -1)$, $(1, -1)$ and $(-1, 1)$ of the square $\square$ to the vertices $(0, 0)$, $(1, 0)$ and $(0, 1)$ of the triangle $\triangle$, respectively, while the middle point $(1/2, 1/2)$ of the hypotenuse is the image of the vertex $(1, 1)$ of $\square$. In other words, this mapping deforms two edges ($\xi = 1$ and $\eta = 1$) of $\square$ into the hypotenuse of $\triangle$, see Fig. 1 for illustration.

Under this mapping, we have

$$\frac{\partial x}{\partial \xi} = \frac{3-\eta}{8}, \quad \frac{\partial x}{\partial \eta} = -\frac{1+\xi}{8}, \quad \frac{\partial y}{\partial \xi} = -\frac{1+\eta}{8}, \quad \frac{\partial y}{\partial \eta} = \frac{3-\xi}{8}, \tag{2.3}$$

and the Jacobian is given by

$$J = \det\left(\frac{\partial(x, y)}{\partial(\xi, \eta)}\right) = \frac{2-\xi-\eta}{16} = \frac{\sqrt{(x-y)^2 + 4(1-x-y)}}{8} := \frac{\chi}{8}. \tag{2.4}$$

For convenience of presentation, we use the notation:

$$\widetilde{\nabla} = (\partial_\xi, \partial_\eta), \quad \widetilde{\nabla}^\perp = (-\partial_\eta, \partial_\xi), \quad \widetilde{\nabla}^\intercal = (1-\xi)\partial_\xi - (1-\eta)\partial_\eta, \tag{2.5}$$

where we put "$\widetilde{\ }$" to distinguish them from the differential operators in (x, y).

In what follows, let $\omega > 0$ be a generic weight function on $\Omega = \triangle$ or $\square$. The weighted Sobolev space $H^r_\omega(\Omega)$ with $r \geq 0$ is defined as in Adams [1], and its norm and semi-norm are denoted by $\|\cdot\|_{r,\omega,\Omega}$ and $|\cdot|_{r,\omega,\Omega}$, respectively. In particular, if $r = 0$, we denote the inner product and norm of $L^2_\omega(\Omega)$ by $(\cdot,\cdot)_{\omega,\Omega}$ and $\|\cdot\|_{\omega,\Omega}$, respectively. Moreover, if $\omega \equiv 1$, we drop it from the notation.

Given $u : \triangle \to \mathbb{R}$, we define the transformed function: $\tilde{u}(\xi, \eta) = (u \circ T)(\xi, \eta) = u(x, y)$. Then for any $u, v \in L^2(\triangle)$, we have

$$(u, v)_\triangle = \iint_\triangle u(x, y)v(x, y)\mathrm{d}x\mathrm{d}y = \iint_\square \tilde{u}(\xi, \eta)\tilde{v}(\xi, \eta)J\ \mathrm{d}\xi\mathrm{d}\eta. \tag{2.6}$$

Moreover, one verifies that

$$\nabla u = (\partial_x u, \partial_y u) = \chi^{-1}\big(2(\widetilde{\nabla}\cdot\tilde{u}) + (\widetilde{\nabla}^{\intercal}\tilde{u}),\ 2(\widetilde{\nabla}\cdot\tilde{u}) - (\widetilde{\nabla}^{\intercal}\tilde{u})\big), \tag{2.7}$$

and

$$(\nabla u, \nabla v)_{\triangle} = \iint_{\square} \big(\widetilde{\nabla}\cdot\tilde{u}\big)\big(\widetilde{\nabla}\cdot\tilde{v}\big)\chi^{-1}\mathrm{d}\xi\mathrm{d}\eta + \frac{1}{4}\iint_{\square}\big(\widetilde{\nabla}^{\intercal}\tilde{u}\big)\big(\widetilde{\nabla}^{\intercal}\tilde{v}\big)\chi^{-1}\mathrm{d}\xi\mathrm{d}\eta. \tag{2.8}$$

We observe from (2.7)–(2.8) that if ∇u is continuous at the middle point $(1/2, 1/2)$ of the hypotenuse of $\triangle$, there automatically holds (note: $(\widetilde{\nabla}^{\intercal}\tilde{u})|_{(1,1)} = 0$):

$$\big(\widetilde{\nabla}\cdot\tilde{u}\big)|_{(1,1)} = \left(\frac{\partial\tilde{u}}{\partial\xi} + \frac{\partial\tilde{u}}{\partial\eta}\right)\Big|_{(1,1)} = 0, \tag{2.9}$$

which is referred to as the consistency condition, and can be viewed as an analogy of the pole condition in the polar/spherical coordinates. In general, we have to build the condition (2.9) in the approximation space so as to obtain high-order accuracy, which therefore results in the reduction of dimension and modification of the usual basis functions (cf. [27]).

One important goal of this paper is to demonstrate that this singularity can be removed, thanks to the observation:

$$\iint_{\square}\frac{1}{2-\xi-\eta}\,\mathrm{d}\xi\mathrm{d}\eta = 4\ln 2, \tag{2.10}$$

which implies that for any $f \in C(\overline{\square})$,

$$\Big|\iint_{\square}\frac{f(\xi,\eta)}{2-\xi-\eta}\,\mathrm{d}\xi\mathrm{d}\eta\Big| \le 4M\ln 2, \tag{2.11}$$

where $M = \max_{\overline{\square}}|f(\xi,\eta)|$. In particular, the coordinate singularity can be eliminated, if f is a polynomial on $\square$ (see Section 3.2).

Now, we present other important features of this mapping. Hereafter, let $I = (-1, 1)$, and for any integer $N \ge 1$, let $P_N(I)$ be the set of all algebraic polynomials of degree at most N. Denote by

$$\mathcal{P}_N(\triangle) := \mathrm{span}\big\{x^i y^j : 0 \le i + j \le N\big\}, \quad \mathcal{Q}_N(\square) := (P_N(I))^2. \tag{2.12}$$

The following property shows a characterization of $\mathcal{Q}_N(\square)$ in terms of the polynomial space on $\triangle$.

Proposition 2.1 *Let $\mathcal{P}_k(\triangle)\circ T = \{P\circ T : P \in \mathcal{P}_k(\triangle)\}$. We have*

(i) $\mathcal{P}_N(\triangle)\circ T \subset \mathcal{Q}_N(\square)$.
(ii) $\mathcal{Q}_N(\square) = \big(\mathcal{P}_N(\triangle)\circ T\big) \oplus \chi\big(\mathcal{P}_{N-1}(\triangle)\circ T\big)$.

Here, T is the rectangle–triangle transform defined by (2.1), and $\chi = (2-\xi-\eta)/2$.

Proof We find from (2.1) that for $0 \le i + j \le N$,

$$x^i y^j = \Big(\frac{1+\xi}{2}\Big)^i\Big(\frac{3-\eta}{4}\Big)^i\Big(\frac{3-\xi}{4}\Big)^j\Big(\frac{1+\eta}{2}\Big)^j \in \mathcal{Q}_N(\square).$$

This leads to the inclusion in (i).

We see that for $0 \le i + j \le N - 1$,

$$x^i y^j \chi = \Big(\frac{1+\xi}{2}\Big)^i \Big(\frac{3-\eta}{4}\Big)^i \Big(\frac{3-\xi}{4}\Big)^j \Big(\frac{1+\eta}{2}\Big)^j \frac{2-\xi-\eta}{2} \in \mathcal{Q}_N(\square),$$

which implies $\chi\big(\mathcal{P}_{N-1}(\triangle) \circ T\big) \subset \mathcal{Q}_N(\square)$.

It remains to prove $\mathcal{Q}_N(\square) \subset \big(\mathcal{P}_N(\triangle) \circ T\big) \oplus \chi\big(\mathcal{P}_{N-1}(\triangle) \circ T\big)$, which we will show by induction. Firstly, by (2.2), it is true for ξ, η, so is $\xi\eta$, since $\xi\eta = 5 - 4x - 4y - 2\chi$. Now, assume that it holds for $\xi^i\eta^j$ with $0 \le i, j \le N-1$. Then, for $0 \le i, j \le N$, we find that $\xi^N\eta^j = \xi(\xi^{N-1}\eta^j)$, $\xi^i\eta^N = \eta(\xi^i\eta^{N-1})$, and $\xi^N\eta^N = (\xi\eta)(\xi^{N-1}\eta^{N-1})$ are all of the form $(a+bx+cy+d\chi)(p(x,y)+q(x,y)\chi)$, where a, b, c, d are constants, $p \in \mathcal{P}_{N-1}(\triangle)$ and $q \in \mathcal{P}_{N-2}(\triangle)$. It is apparent that

$$\begin{aligned}(a+bx+cy+d\chi)(p+q\chi) &= (a+bx+cy)p + dp\chi + (a+bx+cy)q\chi + dq\chi^2 \\ &\overset{(2.2)}{=} (a+bx+cy)p + d\big((x-y)^2 + 4(1-x-y)\big)q + \big(dp + (a+bx+cy)q\big)\chi.\end{aligned}$$

Since $(a+bx+cy)p, d\chi^2 q \in \mathcal{P}_N(\triangle)$ and $dp, (a+bx+cy)q \in \mathcal{P}_{N-1}(\triangle)$, we have

$$\xi^N\eta^j, \xi^i\eta^N, \xi^N\eta^N \in \big(\mathcal{P}_N(\triangle) \circ T\big) \oplus \chi\big(\mathcal{P}_{N-1}(\triangle) \circ T\big),$$

for all $0 \le i, j \le N$. This completes the induction. □

Proposition 2.2 *For any $u \in H^1(\triangle)$, we have*

$$\begin{aligned}\frac{\sqrt{6}}{4}\big\|\widetilde{\nabla}\cdot\tilde{u}\big\|_{\chi^{-1},\square} + \frac{1}{4}\big\|\widetilde{\nabla}^\perp\cdot\tilde{u}\big\|_{\chi,\square} &\le \big\|\nabla u\big\|_{\triangle} \le \frac{\sqrt{5}}{2}\big\|\widetilde{\nabla}\cdot\tilde{u}\big\|_{\chi^{-1},\square} \\ &\quad + \frac{1}{2}\big\|\widetilde{\nabla}^\perp\cdot\tilde{u}\big\|_{\chi,\square},\end{aligned} \tag{2.13}$$

where $\chi = (2-\xi-\eta)/2$, $\tilde{u} = u \circ T$ and the differential operators are defined in (2.5).

Proof By (2.8), we have

$$\big\|\nabla u\big\|_{\triangle}^2 = \big\|\widetilde{\nabla}\cdot\tilde{u}\big\|_{\chi^{-1},\square}^2 + \frac{1}{4}\big\|\widetilde{\nabla}^{\intercal}\tilde{u}\big\|_{\chi^{-1},\square}^2.$$

Then using the identity:

$$\widetilde{\nabla}^{\intercal}\tilde{u} = (1-\xi)\partial_\xi\tilde{u} - (1-\eta)\partial_\eta\tilde{u} = \frac{1}{2}\big(2\chi(\widetilde{\nabla}^\perp\cdot\tilde{u}) - (\xi-\eta)(\widetilde{\nabla}\cdot\tilde{u})\big),$$

we obtain

$$\big\|\nabla u\big\|_{\triangle}^2 = \big\|\widetilde{\nabla}\cdot\tilde{u}\big\|_{\chi^{-1},\square}^2 + \frac{1}{16}\big\|2\chi(\widetilde{\nabla}^\perp\cdot\tilde{u}) - (\xi-\eta)(\widetilde{\nabla}\cdot\tilde{u})\big\|_{\chi^{-1},\square}^2. \tag{2.14}$$

As $|\xi - \eta| \le 2$, we get

$$\big\|2\chi(\widetilde{\nabla}^\perp\cdot\tilde{u}) - (\xi-\eta)(\widetilde{\nabla}\cdot\tilde{u})\big\|_{\chi^{-1},\square}^2 \le 4\big\|\widetilde{\nabla}^\perp\cdot\tilde{u}\big\|_{\chi,\square}^2 + 4\big\|\widetilde{\nabla}\cdot\tilde{u}\big\|_{\chi^{-1},\square}^2.$$

Thus, the upper bound of (2.13) is a consequence of (2.14).

It is clear that

$$-4(\xi-\eta)\chi(\widetilde{\nabla}^\perp\cdot\tilde{u})(\widetilde{\nabla}\cdot\tilde{u}) \ge -\big(2\chi^2|\widetilde{\nabla}^\perp\cdot\tilde{u}|^2 + 2(\xi-\eta)^2|\widetilde{\nabla}\cdot\tilde{u}|^2\big).$$

Thus,

$$\begin{aligned}\big(2\chi(\widetilde{\nabla}^{\perp}\cdot\tilde{u})-(\xi-\eta)(\widetilde{\nabla}\cdot\tilde{u})\big)^2 &\geq 2\chi^2|\widetilde{\nabla}^{\perp}\cdot\tilde{u}|^2-(\xi-\eta)^2|\widetilde{\nabla}\cdot\tilde{u}|^2\\ &\geq 2\chi^2|\widetilde{\nabla}^{\perp}\cdot\tilde{u}|^2-4|\widetilde{\nabla}\cdot\tilde{u}|^2,\end{aligned}$$

which implies

$$\big\|2\chi(\widetilde{\nabla}^{\perp}\cdot\tilde{u})-(\xi-\eta)(\widetilde{\nabla}\cdot\tilde{u})\big\|^2_{\chi^{-1},\square}\geq 2\big\|\widetilde{\nabla}^{\perp}\cdot\tilde{u}\big\|^2_{\chi,\square}-4\big\|\widetilde{\nabla}\cdot\tilde{u}\big\|^2_{\chi^{-1},\square}.$$

Therefore, the lower bound of (2.13) follows from (2.14) and the fundamental inequality: $A^2+B^2\geq(A+B)^2/2$. □

Remark 2.1 We find from Proposition 2.2 that under the rectangle–triangle mapping (2.1), the space $H^1(\triangle)$ is mapped to the weighted space on $\square$:

$$\widetilde{H}^1_{\chi}(\square):=\big\{\tilde{u}\in L^2_{\chi}(\square):\widetilde{\nabla}\cdot\tilde{u}\in L^2_{\chi^{-1}}(\square),\widetilde{\nabla}^{\perp}\cdot\tilde{u}\in L^2_{\chi}(\square)\big\},\tag{2.15}$$

and vice verse. □

2.2 Some new perspectives and a comparison study

Next, we have some insights of the rectangle–triangle mapping and compare it with the Duffy's transform [12].

Firstly, the transform (2.1) is a special case of the general mapping $T_\theta:\square\mapsto\triangle$:

$$(x,y)=\left(\frac{1+\xi}{2}\frac{2-(1-\theta)(1+\eta)}{2},\frac{1+\eta}{2}\frac{2-\theta(1+\xi)}{2}\right),\quad\forall(\xi,\eta)\in\square,\tag{2.16}$$

with $\theta=1/2$. We see that this mapping pulls the hypotenuse of $\triangle$ into two edges of $\square$ at the point $(\theta,1-\theta)$. The limiting case with $\theta=0$ reduces to the Duffy's transform: $T_D:\square\mapsto\triangle$:

$$x=\frac{1}{4}(1+\xi)(1-\eta),\quad y=\frac{1}{2}(1+\eta),\quad\forall\,(\xi,\eta)\in\square,\tag{2.17}$$

with the inverse transform: $T_D^{-1}:\triangle\mapsto\square$:

$$\xi=\frac{2x}{1-y}-1,\quad\eta=2y-1,\quad\forall\,(x,y)\in\triangle.$$

It collapses one edge, $\eta=1$, of $\square$ into the vertex $(0,1)$ of $\triangle$. As the singular vertex corresponds to one edge, the Duffy's transform is not a one-to-one mapping, as opposite to (2.1). This results in a large portion of mapped LGL points clustered near the singular vertex of $\triangle$ (see Fig. 1d). The Jacobian of (2.17) is $J=(1-\eta)/8$, and we have

$$\nabla u=\Big(\frac{4}{1-\eta}\partial_\xi\tilde{u},\frac{2(1+\xi)}{1-\eta}\partial_\xi\tilde{u}+2\partial_\eta\tilde{u}\Big).\tag{2.18}$$

Different from (2.9), the corresponding consistency condition for the Duffy's transform becomes $\partial_\xi\tilde{u}(\xi,1)=0$. In a distinct contrast with (2.10), the integral

$$\iint_{\square}\frac{1}{1-\eta}\,\mathrm{d}\xi\mathrm{d}\eta=\infty.\tag{2.19}$$

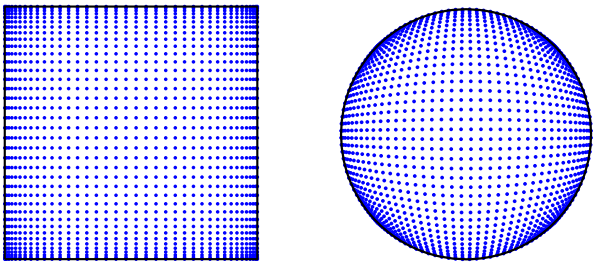

Fig. 2 *Left* Tensorial Legendre–Gauss–Lobatto points on the square. *Right* The corresponding mapped LGL points on the unit disc

Consequently, the consistency condition has to be built in the approximation space, and much care has to be taken to deal with this singularity for the Duffy's transform-based methods in terms of implementation and analysis.

Secondly, the nature of the point singularity of (2.1) is reminiscent to that of the Gordon-Hall mapping [14], which maps the reference square to the unit disc via

$$x = \frac{\xi}{\sqrt{2}}\sqrt{2-\eta^2}, \quad y = \frac{\eta}{\sqrt{2}}\sqrt{2-\xi^2}, \quad \forall\,(\xi,\eta) \in \square,$$

and whose Jacobian is $(2-\xi^2-\eta^2)/\sqrt{(2-\xi^2)(2-\eta^2)}$. It is clear that this transform induces singularities at the four vertices of the reference square (cf. Fig. 2). It is worthwhile to point out that the collocation scheme on the unit disc using this mapping was discussed in [18], and this mapping technique was further examined in [2].

In addition, we find that the rectangle–triangle transform (2.1) can be derived from the following symmetric mapping on $\square$:

$$\hat{x} = \xi + \eta, \quad \hat{y} = \xi\eta, \quad \forall\,(\xi,\eta) \in \square. \tag{2.20}$$

It transforms any symmetric polynomial in (ξ,η) to a polynomial in $(\hat{x},\hat{y})$, so it is referred to as a symmetric mapping [37]. One verifies that the image of this mapping is the curvilinear triangle (see Fig. 3b):[1]

$$\Omega = \big\{(\hat{x},\hat{y}) : 1-\hat{x}+\hat{y},\ 1+\hat{x}+\hat{y},\ \hat{x}^2-4\hat{y} > 0\big\}.$$

As the symmetric mapping (2.20), denoted by $\widehat{T} : \square \mapsto \Omega$, cannot distinguish the images of (ξ,η) and (η,ξ), it is not one-to-one. To amend this, one may restrict the domain of $\widehat{T}$ to the upper triangle, denoted by $\triangle_{\text{up}}$, in $\square$ (see Fig. 3a), and interestingly, the square of maximum area contained in this subdomain is one-to-one mapped to the triangle of maximum area included in the curvilinear triangle Ω, that is,

$$\widehat{T} : \widehat{\square} := (-1,0)\times(0,1) \longmapsto \widehat{\triangle} := \big\{(\hat{x},\hat{y}) : |\hat{x}| < 1+\hat{y} < 1\big\}, \tag{2.21}$$

is a bijective mapping (see the shaded parts in Fig. 3a–b). For clarity of presentation, we denote the coordinate of any point in $\widehat{\square}$ by $(\hat{\xi},\hat{\eta})$. It is clear that the reference

[1] It is worthwhile to note that thanks to the symmetric mapping $\widehat{T} : \square \mapsto \Omega$, Xu [39] discovered the first example of multivariate Gauss quadrature.

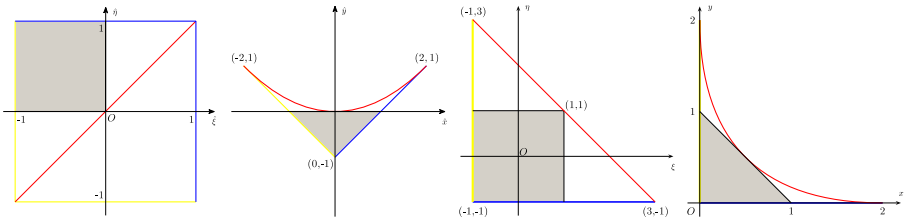

Fig. 3 **a** The reference *square* $\square$, the *upper triangle* $\triangle_{\text{up}} = \{(x, y) : -1 < x < y < 1\}$ and the *square* $\widehat{\square}$ (*shaded*). **b** The image Ω (resp. $\widehat{\triangle}$ (*shaded*)) of the symmetric mapping $\widehat{T}$ whose domain is $\triangle_{\text{up}}$ (resp. $\widehat{\square}$ (*shaded*)). **c** Domains obtained from $\widehat{\square}$ and the *upper triangle* $\triangle_{\text{up}}$ in **a** by the affine mapping F_1. **d** Domains obtained from $\widehat{\triangle}$ and Ω in **b** by the affine mapping F_2

square $\square$ and $\widehat{\square}$ are connected by the affine mapping: $F_1 : \square \mapsto \widehat{\square}$, of the form (see the shaded parts of Fig. 3a, c):

$$\hat{\xi} = \frac{\xi - 1}{2}, \quad \hat{\eta} = \frac{1 - \eta}{2}, \quad \forall (\xi, \eta) \in \square, \tag{2.22}$$

and the affine mapping: $F_2 : \widehat{\triangle} \mapsto \triangle$, takes the form (see the shaded parts of Fig. 3b, d):

$$x = \frac{1}{2}(\hat{y} + \hat{x} + 1), \quad y = \frac{1}{2}(\hat{y} - \hat{x} + 1), \quad \forall (\hat{x}, \hat{y}) \in \widehat{\triangle}. \tag{2.23}$$

In summary, we have $\square \overset{F_1}{\longmapsto} \widehat{\square} \overset{\widehat{T}}{\longmapsto} \widehat{\triangle} \overset{F_2}{\longmapsto} \triangle$. Remarkably, this composite mapping is identical to the rectangle–triangle mapping (2.1), i.e., $T = F_1 \circ \widehat{T} \circ F_2$.

3 Basis functions and computation of the stiffness matrix

We introduce in this section the modal and nodal basis functions on triangles, and present a fast and accurate algorithm for computing the stiffness matrix with a focus on how to deal with the singularity (cf. (2.10)–(2.11)).

3.1 Modal basis

Let $I = (-1, 1)$ as before. We define the space

$$Y_N(\triangle) = \mathcal{Q}_N(\square) \circ T^{-1} = (P_N(I))^2 \circ T^{-1}, \tag{3.1}$$

which consists of the images of the tensor-product polynomials on $\square$ under the inverse mapping T^{-1} defined in (2.2). As a direct consequence of Proposition 2.1 (ii), we have

$$Y_N(\triangle) = \mathcal{P}_N(\triangle) \oplus \chi \mathcal{P}_{N-1}(\triangle), \tag{3.2}$$

where $\chi = \sqrt{(x - y)^2 + 4(1 - x - y)}$, and we recall that $\mathcal{P}_N(\triangle)$ is the set of polynomials on $\triangle$ of total degree at most N. This implies that $Y_N(\triangle)$ contains not only polynomials, but also special irrational functions: $\chi\phi$ for any $\phi \in \mathcal{P}_{N-1}(\triangle)$.

Define the modes

$$\phi_0(\zeta)=\frac{1-\zeta}{2},\quad \phi_k(\zeta)=\frac{1-\zeta^2}{4}J_{k-1}^{1,1}(\zeta),\quad 1\le k\le N-1,\quad \phi_N(\zeta)=\frac{1+\zeta}{2}, \tag{3.3}$$

where $J_k^{1,1}$ is the Jacobi polynomial of degree k (cf. [35]). It is clear that $\{\phi_k\}_{k=0}^N$ forms a basis of $P_N(I)$, and we have

$$\mathcal{Q}_N(\square)=\operatorname{span}\big\{\Phi_{kl}:\Phi_{kl}(\xi,\eta)=\phi_k(\xi)\phi_l(\eta),\ 0\le k,l\le N\big\}. \tag{3.4}$$

It is a commonly used C^0-modal basis for QSEM, which enjoys a distinct separation of the interior and boundary modes (including vertex and edge modes): all interior modes (i.e., Φ_{kl}, for $0<k,l<N$) are zero on the boundary; the vertex modes (i.e., Φ_{kl}, for $k,l\in\{0,N\}$) have a unit magnitude at one vertex and are zero at all other vertices; and the edge modes (i.e., Φ_{kl}, for all other k,l) only have magnitude along one edge and are zero at all vertices and at all other edges.

In view of (3.1) and (3.4), we obtain the modal basis for $Y_N(\triangle)$:

$$Y_N(\triangle)=\operatorname{span}\big\{\Psi_{kl}:\Psi_{kl}(x,y)=\Phi_{kl}\circ T^{-1},\ 0\le k,l\le N\big\}. \tag{3.5}$$

3.2 Computation of the stiffness matrix

Though the singular integral of (2.11)-type has a finite value, some efforts are needed to compute such integrals in a fast and stable manner. Next, we devise an efficient algorithm for this purpose.

Let L_k be the Legendre polynomial of degree $k\ge 0$, and recall that (see e.g., [35]) for $k\ge 1$,

$$\left(1-\zeta^2\right)J_{k-1}^{1,1}(\zeta)=\frac{2k}{2k+1}\big(L_{k-1}(\zeta)-L_{k+1}(\zeta)\big), \tag{3.6}$$

$$(2k+1)L_k(\zeta)=L'_{k+1}(\zeta)-L'_{k-1}(\zeta), \tag{3.7}$$

$$\zeta L_k(\zeta)=\frac{k}{2k+1}L_{k-1}(\zeta)+\frac{k+1}{2k+1}L_{k+1}(\zeta). \tag{3.8}$$

Thus, we have

$$\phi_0'(\zeta)=-\frac{1}{2}L_0(\zeta)=-\phi_N'(\zeta),\quad \phi_k'(\zeta)=-\frac{k}{2}L_k(\zeta),\quad 1\le k\le N-1. \tag{3.9}$$

By (2.5), (2.7) and (3.4),

$$\begin{aligned}\chi\,\partial_x\Psi_{kl}&=2\big(\phi_k'(\xi)\phi_l(\eta)+\phi_k(\xi)\phi_l'(\eta)\big)+\big[(1-\xi)\phi_k'(\xi)\phi_l(\eta)-(1-\eta)\phi_k(\xi)\phi_l'(\eta)\big],\\ \chi\,\partial_y\Psi_{kl}&=2\big(\phi_k'(\xi)\phi_l(\eta)+\phi_k(\xi)\phi_l'(\eta)\big)-\big[(1-\xi)\phi_k'(\xi)\phi_l(\eta)-(1-\eta)\phi_k(\xi)\phi_l'(\eta)\big].\end{aligned} \tag{3.10}$$

Thanks to (3.6)–(3.10), $\chi\,\partial_x\Psi_{kl}$ and $\chi\,\partial_y\Psi_{kl}$ can be represented by a linear combination of $\{L_{k\pm i}(\xi)L_{l\pm j}(\eta)\}_{i,j=0,1}$. In view of this, we can evaluate the entries of the stiffness matrix by computing the integrals of the product of Legendre polynomials:

$$s_{kl}^{k'l'} := \iint_{\triangle} \nabla\Psi_{kl}\cdot\nabla\Psi_{k'l'}\,\mathrm{d}x\mathrm{d}y \quad\longleftrightarrow\quad \iint_{\square} \frac{L_i(\xi)L_j(\eta)L_{i'}(\xi)L_{j'}(\eta)}{2-\xi-\eta}\,\mathrm{d}\xi\mathrm{d}\eta := a_{ij}^{i'j'}. \tag{3.11}$$

Using the fact that the product L_mL_n can be represented by $\{L_p\}_{p=0}^{m+n}$:

$$L_m(\xi)L_n(\xi) = \sum_{p=0}^{m+n} c_p^{mn} L_p(\xi), \tag{3.12}$$

where the expansion coefficient $\{c_p^{mn}\}$ can be found in e.g., [21], we obtain

$$a_{ij}^{i'j'} = \sum_{p=0}^{i+i'}\sum_{q=0}^{j+j'} c_p^{ii'}c_q^{jj'}\hat{a}_{pq}, \quad \text{where } \hat{a}_{pq} = \iint_{\square} \frac{L_p(\xi)L_q(\eta)}{2-\xi-\eta}\,\mathrm{d}\xi\mathrm{d}\eta. \tag{3.13}$$

Now, we describe how to compute $\{\hat{a}_{pq}\}$ in a fast and accurate manner. This essentially relies on the following recurrence relation.

Lemma 3.1 *We have*

$$\frac{\hat{a}_{p,q+1}-\hat{a}_{p,q-1}}{2q+1} = \frac{\hat{a}_{p+1,q}-\hat{a}_{p-1,q}}{2p+1}, \quad \forall\, p,q\geq 1. \tag{3.14}$$

Proof The statement is true for $p=q\geq 1$. Since $\hat{a}_{pq}=\hat{a}_{qp}$, it suffices to show that the recurrence is valid for $p>q\geq 1$.

We start with recalling the Legendre functions of the second kind (see [35, Formula (4.61.4)]):

$$Q_n(x) = \frac{1}{2}\int_{-1}^{1}\frac{L_n(t)}{x-t}\,\mathrm{d}t, \quad n\geq 1; \quad Q_0(x) = \frac{1}{2}\ln\frac{x+1}{x-1}, \quad \forall x>1, \tag{3.15}$$

and the important identity (see [35, Formula (4.62.1)]):

$$\begin{aligned} Q_n(x) &= \frac{1}{2}\Big(\ln\frac{x+1}{x-1}\Big)L_n(x) - \frac{1}{2}\int_{-1}^{1}\frac{L_n(x)-L_n(t)}{x-t}\,\mathrm{d}t \\ &= \frac{1}{2}\Big(\ln\frac{x+1}{x-1}\Big)L_n(x) - \tilde{L}_{n-1}(x). \end{aligned} \tag{3.16}$$

Here, $\tilde{L}_n$ is the Legendre polynomial of the second kind, satisfying

$$\tilde{L}_n(x) = \frac{2n+1}{n+1}x\tilde{L}_{n-1}(x) - \frac{n}{n+1}\tilde{L}_{n-2}(x), \quad n\geq 1; \quad \tilde{L}_{-1}(x)=0, \quad \tilde{L}_0(x)=1, \tag{3.17}$$

which follows from (3.16) and [35, Formula (4.62.13)] directly.

Using (3.15)–(3.17) and the orthogonality of the Legendre polynomials, we find that for $p > q \geq 1$,

$$\begin{aligned}\hat{a}_{pq} &= \int_{-1}^{1}\int_{-1}^{1} \frac{L_p(\xi)L_q(\eta)}{2-\xi-\eta}\,\mathrm{d}\xi\,\mathrm{d}\eta = 2\int_{-1}^{1} Q_q(2-\xi)L_p(\xi)\,\mathrm{d}\xi \\ &= \int_{-1}^{1}\left[\left(\ln\frac{3-\xi}{1-\xi}\right)L_q(2-\xi) - 2\tilde{L}_{q-1}(2-\xi)\right]L_p(\xi)\,\mathrm{d}\xi \\ &= \int_{-1}^{1}\left(\ln\frac{3-\xi}{1-\xi}\right)L_q(2-\xi)L_p(\xi)\,\mathrm{d}\xi. \end{aligned} \tag{3.18}$$

Thus, we have from (3.7) and integration by parts that

$$\begin{aligned}\frac{\hat{a}_{p,q+1}-\hat{a}_{p,q-1}}{2q+1} &= \int_{-1}^{1}\left(\ln\frac{3-\xi}{1-\xi}\right)\frac{L_{q+1}(2-\xi)-L_{q-1}(2-\xi)}{2q+1}L_p(\xi)\,\mathrm{d}\xi \\ &= \int_{-1}^{1}\left(\ln\frac{3-\xi}{1-\xi}\right)\frac{L_{q+1}(2-\xi)-L_{q-1}(2-\xi)}{2q+1} \\ &\quad\times\left[\frac{L_{p+1}(\xi)-L_{p-1}(\xi)}{2p+1}\right]'\mathrm{d}\xi \\ &= -\int_{-1}^{1}\left[\left(\ln\frac{3-\xi}{1-\xi}\right)\frac{L_{q+1}(2-\xi)-L_{q-1}(2-\xi)}{2q+1}\right]' \\ &\quad\times\frac{L_{p+1}(\xi)-L_{p-1}(\xi)}{2p+1}\,\mathrm{d}\xi.\end{aligned}$$

Working out the derivative, we obtain

$$\begin{aligned}&\frac{\hat{a}_{p,q+1}-\hat{a}_{p,q-1}}{2q+1} \\ &\overset{(3.7)}{=} \int_{-1}^{1}\left[L_q(2-\xi)\ln\left(\frac{3-\xi}{1-\xi}\right) - \frac{L_{q+1}(2-\xi)-L_{q-1}(2-\xi)}{(q+1/2)(3-\xi)(1-\xi)}\right] \\ &\quad\times\frac{L_{p+1}(\xi)-L_{p-1}(\xi)}{2p+1}\,\mathrm{d}\xi \\ &\overset{(3.18)}{=} \frac{\hat{a}_{p+1,q}-\hat{a}_{p-1,q}}{2p+1} - \int_{-1}^{1}\frac{L_{q+1}(2-\xi)-L_{q-1}(2-\xi)}{(q+1/2)(3-\xi)(1-\xi)}\,\frac{L_{p+1}(\xi)-L_{p-1}(\xi)}{2p+1}\,\mathrm{d}\xi \\ &\overset{(3.6)}{=} \frac{\hat{a}_{p+1,q}-\hat{a}_{p-1,q}}{2p+1} + \frac{1}{2pq}\int_{-1}^{1} J_{q-1}^{1,1}(2-\xi)J_{p-1}^{1,1}(\xi)(1-\xi^2)\,\mathrm{d}\xi \\ &= \frac{\hat{a}_{p+1,q}-\hat{a}_{p-1,q}}{2p+1},\end{aligned}$$

where we used the fact $p > q$ and the orthogonality of Jacobi polynomials in the last step. □

We summarize the algorithm as follows.

Algorithm for computing $\{\hat{a}_{pq}\}_{p,q=0}^{N}$

1. Initialization
   (a) For $p = 0, 1, \cdots, 2N$, compute $\hat{a}_{p0}$;
   (b) For $p = 1, 2, \cdots, 2N-1$, compute $\hat{a}_{p1}$.
2. For $q = 2, 3, \cdots, N$,
   For $p = q, \cdots, 2N - q$,
   $$\hat{a}_{pq} = \hat{a}_{p,q-2} + \frac{2q-1}{2p+1}(\hat{a}_{p+1,q-1} - \hat{a}_{p-1,q-1}), \tag{3.19}$$
   Endfor of p, q.
3. Set $\hat{a}_{pq} = \hat{a}_{qp}$ for all $0 \le p < q < N$.

We describe below the details for computing the initial values.

- We find from (3.18) that

$$\begin{aligned}\hat{a}_{p0} &= \int_{-1}^{1} L_p(\xi) \ln \frac{3-\xi}{1-\xi}\, \mathrm{d}\xi \\ &= \int_{-1}^{1} L_p(\xi) \ln \frac{3-\xi}{2}\, \mathrm{d}\xi + \int_{-1}^{1} L_p(\xi) \ln \frac{2}{1-\xi}\, \mathrm{d}\xi := \alpha_p + \beta_p. \end{aligned} \tag{3.20}$$

  It is clear that $\alpha_0 = 4\ln 2 - 2$, and for $p \ge 1$, we find from (3.7) and integration by parts that

$$\begin{aligned}\alpha_p &= \int_{-1}^{1} L_p(\xi) \ln \frac{3-\xi}{2}\, \mathrm{d}\xi = \frac{\bar{\alpha}_{p+1} - \bar{\alpha}_{p-1}}{2p+1}, \text{ where} \\ \bar{\alpha}_p &= \int_{-1}^{1} \frac{L_p(\xi)}{3-\xi}\, \mathrm{d}\xi, \quad p \ge 0. \end{aligned}$$

  Note that $\{\bar{\alpha}_p\}$ (up to the factor $p + 1/2$) are the Legendre expansion coefficients of the function $1/(3-\xi)$, which merely has a simple pole at $\xi = 3$ in the complex plane, so the use of a Legendre–Gauss quadrature leads to an exponentially accurate approximation (see [38]).

  We find from e.g., [13] that

$$\beta_p = \int_{-1}^{1} L_p(\xi) \ln \frac{2}{1-\xi}\, \mathrm{d}\xi = \begin{cases} 2, & \text{if } p = 0, \\ \dfrac{2}{p(p+1)}, & \text{if } p \ge 1. \end{cases}$$

- Using (3.13), (3.8) and the orthogonality of Legendre polynomials, we find

$$\begin{aligned}\hat{a}_{p1} &= \iint_{\square} \frac{\eta L_p(\xi)}{2-\xi-\eta}\,\mathrm{d}\xi\mathrm{d}\eta \\ &= \iint_{\square} \frac{(2-\xi)L_p(\xi)}{2-\xi-\eta}\,\mathrm{d}\xi\mathrm{d}\eta - \iint_{\square} \frac{(2-\xi-\eta)L_p(\xi)}{2-\xi-\eta}\mathrm{d}\xi\mathrm{d}\eta \\ &= 2\iint_{\square} \frac{L_p(\xi)}{2-\xi-\eta}\,\mathrm{d}\xi\mathrm{d}\eta - \iint_{\square} \frac{\xi L_p(\xi)}{2-\xi-\eta}\,\mathrm{d}\xi\mathrm{d}\eta - \int_{-1}^{1}\left[\int_{-1}^{1} L_p(\xi)\,\mathrm{d}\xi\right]\mathrm{d}\eta \\ &= 2\hat{a}_{p0} - \frac{(p+1)\hat{a}_{p+1,0} + p\hat{a}_{p-1,0}}{2p+1}, \quad p \geq 1. \end{aligned} \tag{3.21}$$

- We see that with an accurate computation of the initial values $\{\hat{a}_{p0}\}$, marching by (3.21) and (3.19) is expected to be stable, since the coefficients of terms $\hat{a}_{pq} - \hat{a}_{p'q}$ are all less than 1. In the left of Fig. 4, we provide a schematic illustration of sweeping the stencils by the algorithm.

Remark 3.1 We see from (3.18) and (3.20) that the rectangle–triangle mapping (2.1) essentially induces logarithmic singularities. By computing the initial values $\{\hat{a}_{p0}\}$ and $\{\hat{a}_{p1}\}$ accurately, we can find $\{\hat{a}_{pq}\}_{p\geq q}$ in a fast and accurate manner. In fact, numerical quadrature of an integrand involving a logarithmic weight function, e.g., $\int_{-1}^{1} f(\xi)\ln\frac{2}{1-\xi}\mathrm{d}\xi$, is of independent interest (see e.g., [13]).

Here, we provide some numerical results to demonstrate the accuracy of computing the initial values $\{\hat{a}_{p0}\}$. Consider

$$\begin{aligned} I_a &:= \int_{-1}^{1} \exp(a(3-\xi))\ln\frac{3-\xi}{1-\xi}\,\mathrm{d}\xi \\ &= \frac{e^{4a}\ln 2 + e^{2a}[\mathrm{Ei}(2a) - \gamma - \ln(-2a)] - \mathrm{Ei}(4a) + \mathrm{Ei}(2a)}{a}, \end{aligned}$$

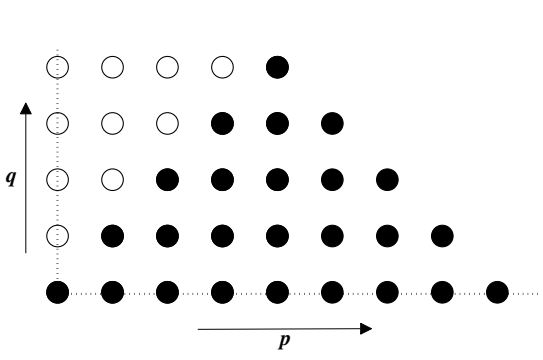

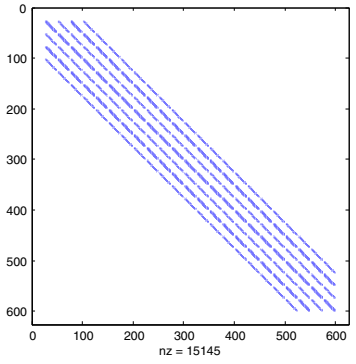

Fig. 4 *Left* Diagram for computing $\{\hat{a}_{pq}\}_{p,q=0}^{N}$ with $N = 2$, where the stencils marked by "•" are marched via Steps 1–2 in the **Algorithm**, and those marked by "○" are obtained by the symmetric property in Step 3. *Right* Sparsity pattern plot of the mass matrix involving the interior basis with $N = 24$

where the constant $a < 0$, $\mathrm{Ei}(x)$ is the exponential integral function, and $\gamma(\approx 0.5772)$ is the Euler–Mascheroni constant (see e.g., [15]).

We tabulate in Table 1 the relative errors for various a and N, which shows a typical spectral accuracy as expected. □

Remark 3.2 As a quick note, the mass matrix under this basis is sparse (see Fig. 4 (right)). Indeed, by (2.6),

$$(u, v)_{\triangle} = \frac{1}{8}\iint_{\square} \tilde{u}\tilde{v}\,\mathrm{d}\xi\mathrm{d}\eta - \frac{1}{16}\iint_{\square} \xi\tilde{u}\tilde{v}\,\mathrm{d}\xi\mathrm{d}\eta - \frac{1}{16}\iint_{\square} \eta\tilde{u}\tilde{v}\,\mathrm{d}\xi\mathrm{d}\eta, \tag{3.22}$$

so we claim this from (3.8) and the orthogonality of the Legendre polynomials. □

Remark 3.3 With an additional affine mapping, any triangular element $\triangle_{\text{any}}$ can be transformed to the reference square $\square$. It is important to point out that the stiffness and mass matrices on $\triangle_{\text{any}}$ can be precomputed in a similar fashion as above. To justify this, we consider a general triangle $\triangle_{\text{any}}$ with vertices $V_i = (x_i, y_i)$, $i = 1, 2, 3$. Like (2.1), we have the mapping from $\square$ to $\triangle_{\text{any}}$:

$$(x, y) = (x_1, y_1)\frac{(1-\xi)(1-\eta)}{4} + (x_2, y_2)\frac{(1+\xi)(3-\eta)}{8} + (x_3, y_3)\frac{(3-\xi)(1+\eta)}{8}, \tag{3.23}$$

for all $(\xi, \eta) \in \square$. A direct calculation leads to

$$(u, v)_{\triangle_{\text{any}}} = \frac{F}{8}\iint_{\square} \tilde{u}\tilde{v}\,\mathrm{d}\xi\mathrm{d}\eta - \frac{F}{16}\iint_{\square} \xi\tilde{u}\tilde{v}\,\mathrm{d}\xi\mathrm{d}\eta - \frac{F}{16}\iint_{\square} \eta\tilde{u}\tilde{v}\,\mathrm{d}\xi\mathrm{d}\eta, \tag{3.24}$$

and

$$\begin{aligned}(\nabla u, \nabla v)_{\triangle_{\text{any}}} = {} & A\iint_{\square} \big(\widetilde{\nabla}\cdot\tilde{u}\big)\big(\widetilde{\nabla}\cdot\tilde{v}\big)\chi^{-1}\mathrm{d}\xi\mathrm{d}\eta + C\iint_{\square} \big(\widetilde{\nabla}^{\intercal}\tilde{u}\big)\big(\widetilde{\nabla}^{\intercal}\tilde{v}\big)\chi^{-1}\mathrm{d}\xi\mathrm{d}\eta \\ & - B\iint_{\square} \big[\big(\widetilde{\nabla}\cdot\tilde{u}\big)\big(\widetilde{\nabla}^{\intercal}\tilde{v}\big) + \big(\widetilde{\nabla}^{\intercal}\tilde{u}\big)\big(\widetilde{\nabla}\cdot\tilde{v}\big)\big]\chi^{-1}\mathrm{d}\xi\mathrm{d}\eta,\end{aligned} \tag{3.25}$$

where $\chi^{-1} = 2/(2-\xi-\eta)$, the differential operators are defined in (2.5), and the constants are given by

$$\begin{aligned} F &= (x_2 - x_1)(y_3 - y_1) - (x_3 - x_1)(y_2 - y_1) \neq 0, \\ A &= ((x_2 - x_3)^2 + (y_2 - y_3)^2)/(2F), \\ B &= ((x_2 - x_1)^2 + (y_2 - y_1)^2 - (x_3 - x_1)^2 - (y_3 - y_1)^2)/(4F), \\ C &= ((2x_1 - x_2 - x_3)^2 + (2y_1 - y_2 - y_3)^2)/(8F). \end{aligned}$$

Table 1 Relative errors of approximating I_a

N	$a = -1/4$	$a = -1/2$	$a = -3/4$	$a = -1$	$a = -5/4$	$a = -3/2$
6	4.828E−12	5.833E−10	9.291E−09	6.420E−08	2.800E−07	9.111E−07
10	1.096E−15	3.003E−16	7.363E−15	1.352E−13	1.411E−12	9.318E−12
14	1.565E−15	6.006E−16	1.416E−15	5.263E−16	4.828E−16	1.752E−15

In particular, if $\triangle_{\text{any}} = \triangle$, (3.24) and (3.25) (note: $B = 0$) reduce to (2.6) and (2.8), respectively.

As with (3.10), we find from (3.6)–(3.9) that $\widetilde{\nabla} \cdot \Phi_{kl}$ and $\widetilde{\nabla}^{\intercal}\Phi_{kl}$ can be expressed in terms of $\{L_{k\pm i}(\xi)L_{l\pm j}(\eta)\}_{i,j=0,1}$, so the stiffness matrix on $\triangle_{\text{any}}$ can be precomputed by the same algorithm described above. □

3.3 Interpolation, quadrature and nodal basis

Through the general mapping (3.23), the operations (e.g., interpolation, quadrature and numerical differentiation) on a triangular element can be performed on the reference square □.

Hereafter, let $\{\zeta_j\}_{j=0}^N$ be the Legendre–Gauss–Lobatto (LGL) points, i.e., the zeros of $(1-\zeta^2)L'_N(\zeta)$, and let $\{h_j\}_{j=0}^N$ be the associated Lagrangian basis polynomials such that $h_j \in P_N(I), 0 \le j \le N$, and $h_j(\zeta_k) = \delta_{kj}, 0 \le j,k \le N$ (where δ_{kj} is the Kronecker delta). Given $v \in C(\bar{I})$, the one-dimensional polynomial interpolant of v is

$$\left(I_N^{\zeta} v\right)(\zeta) = \sum_{j=0}^{N} v(\zeta_j) h_j(\zeta) \in P_N, \quad \forall\, \zeta \in \bar{I}. \tag{3.26}$$

Recall that the LGL quadrature has degree of precision $2N-1$, i.e.,

$$\int_{-1}^{1} \phi(\zeta)\mathrm{d}\zeta = \sum_{j=0}^{N} \phi(\zeta_j)\omega_j, \quad \forall\, \phi \in P_{2N-1}(I), \tag{3.27}$$

where $\{\omega_j\}_{j=0}^N$ are the LGL quadrature weights.

Given any $u \in C(\bar{\triangle})$, we define the interpolant of u by

$$(\mathbb{I}_N u)(x,y) = (I_N^{\xi} I_N^{\eta} \tilde{u}) \circ T^{-1} = \Big(\sum_{i,j=0}^{n} (u \circ T)(\xi_i, \eta_j) h_i(\xi) h_j(\eta) \Big) \circ T^{-1}, \tag{3.28}$$

where T and T^{-1} are defined in (2.1) and (2.2) as before, and $\{\xi_k = \eta_k = \zeta_k\}_{k=0}^N$. Notice that $\mathbb{I}_N u \in Y_N(\triangle)$.

We also extend the LGL quadrature to define the discrete inner product on $\triangle$ as

$$\langle u, v\rangle_{N,\triangle} = \frac{1}{8} \sum_{i,j=0}^{N} \tilde{u}(\xi_i, \eta_j)\tilde{v}(\xi_i, \eta_j)\chi(\xi_i, \eta_j)\omega_i\omega_j, \tag{3.29}$$

where $\chi = (2-\xi-\eta)/2$. As a consequence of (2.6), (3.27) and (3.1)–(3.2), there holds

$$\langle u, v\rangle_{N,\triangle} = (u, v)_{\triangle}, \quad \forall\, u \cdot v \in Y_{2N-2}(\triangle), \tag{3.30}$$

which also holds for all $u \cdot v \in \mathcal{P}_{2N-2}(\triangle)$.

Since $\{h_k h_l\}_{k,l=0}^N$ forms the nodal basis for $\mathcal{Q}_N(\square)$, we can obtain the nodal basis for $Y_N(\triangle)$:

$$Y_N(\triangle) = \operatorname{span}\big\{\widehat{\Psi}_{kl} : \widehat{\Psi}_{kl}(x,y) = (h_k h_l) \circ T^{-1} \ : \ 0 \le k,l \le N\big\}. \tag{3.31}$$

In view of (3.22), the mass matrix under this nodal basis can be computed easily as usual by tensorial LGL quadrature. However, the direct evaluation of the stiffness

matrix like (3.11) is prohibitive, as there is no recursive way for the computation. In order to surmount this obstacle, we resort to the notion of "discrete transform" (cf. [33]). Like (3.10), we have

$$\begin{aligned}\chi\partial_x\widehat{\Psi}_{kl} &= 2(h_k'(\xi)h_l(\eta)+h_k(\xi)h_l'(\eta))\\ &\quad+[(1-\xi)h_k'(\xi)h_l(\eta)-(1-\eta)h_k(\xi)h_l'(\eta)]\in\mathcal{Q}_N(\square),\\ \chi\partial_y\widehat{\Psi}_{kl} &= 2(h_k'(\xi)h_l(\eta)+h_k(\xi)h_l'(\eta))\\ &\quad-[(1-\xi)h_k'(\xi)h_l(\eta)-(1-\eta)h_k(\xi)h_l'(\eta)]\in\mathcal{Q}_N(\square).\end{aligned}$$

The idea is to transform $\{\chi\partial_x\widehat{\Psi}_{kl}\}_{k,l=0}^N$ and $\{\chi\partial_y\widehat{\Psi}_{kl}\}_{k,l=0}^N$ to $\{L_i(\xi)L_j(\eta)\}_{i,j=0}^N$ via a two-dimensional discrete transform. Then the evaluation boils down to finding $\{a_{ij}^{i'j'}\}$ in (3.11) as before.

4 Estimates of orthogonal projection and interpolation errors

The section is devoted to obtaining error estimates for orthogonal projection and interpolation operators on $Y_N(\triangle)$. These results will be essential for understanding the approximability properties of the basis functions and provide important tools for error analysis of the TSEM for PDEs.

To this end, we denote by c a generic positive constant independent of N and any function.

4.1 Orthogonal projections

We start with considering the projection $\Pi_N : L^2(\triangle)\to Y_N(\triangle)$, defined by

$$\big(\Pi_N u-u,v\big)_\triangle=0,\quad\forall\, v\in Y_N(\triangle).\tag{4.1}$$

Theorem 4.1 *For any $u\in H^r(\triangle)$ with $r\geq 0$, we have*

$$\|\Pi_N u-u\|_\triangle\leq cN^{-r}|u|_{r,\triangle}.\tag{4.2}$$

Proof We have

$$\|\Pi_N u-u\|_\triangle\overset{(4.1)}{=}\inf_{\phi\in Y_N(\triangle)}\|\phi-u\|_\triangle\overset{(3.2)}{\leq}\|\psi-u\|_\triangle,\quad\forall\psi\in\mathcal{P}_N(\triangle).\tag{4.3}$$

Now, we take ψ to be the best L^2-approximation in $\mathcal{P}_N(\triangle)$, denoted by $\pi_N u$. By [25, Theorem 3.3],

$$\begin{aligned}\|\pi_N u-u\|_\triangle &\leq cN^{-r}\left(\sum_{k_1+k_2+k_3=r}\big\|\partial_x^{k_1}\partial_y^{k_2}(\partial_y-\partial_x)^{k_3}u\big\|^2_{\omega^{k_1,k_2,k_3},\triangle}\right)^{1/2}\\ &\leq cN^{-r}|u|_{r,\triangle},\end{aligned}\tag{4.4}$$

where $\omega^{k_1,k_2,k_3}=x^{k_1+k_3}y^{k_2+k_3}(1-x-y)^{k_1+k_2}$ is a Jacobi weight function on $\triangle$. Therefore, the estimate (4.2) follows from (4.3)–(4.4). □

We now turn to the H_0^1-projection: $\Pi_N^{1,0} : H_0^1(\triangle) \to Y_N^0(\triangle) = Y_N(\triangle) \cap H_0^1(\triangle)$, defined by

$$\big(\nabla(\Pi_N^{1,0}u - u), \nabla v\big)_\triangle = 0, \quad \forall\, v \in Y_N^0(\triangle), \tag{4.5}$$

where $H_0^1(\triangle)$ is defined as usual, i.e., the subspace of $H^1(\triangle)$ with functions vanishing on the boundary of $\triangle$.

Theorem 4.2 *For any $u \in H_0^1(\triangle) \cap H^r(\triangle)$ with $r \geq 1$, we have*

$$\|\Pi_N^{1,0}u - u\|_{\mu,\triangle} \leq cN^{\mu-r}|u|_{r,\triangle}, \quad \mu = 0, 1. \tag{4.6}$$

Proof By the Poincaré inequality, we know that the semi-norm $|\cdot|_{1,\triangle}$ is a norm of $H_0^1(\triangle)$. Hence, by the definition (4.5),

$$\|u - \Pi_N^{1,0}\|_{1,\triangle} \leq c|\phi - u|_{1,\triangle} \leq c\|\phi - u\|_{1,\triangle}, \quad \forall\, \phi \in Y_N(\triangle). \tag{4.7}$$

It is known from (3.2) that $\mathcal{P}_N(\triangle) \subset Y_N(\triangle)$, so we can take ϕ to be the orthogonal projection $\pi_N^{1,0} : H_0^1(\triangle) \to \mathcal{P}_N^0(\triangle) = \mathcal{P}_N(\triangle) \cap H_0^1(\triangle)$, defined by

$$\big(\nabla(\pi_N^{1,0}u - u), \nabla v\big)_\triangle = 0, \quad \forall\, v \in \mathcal{P}_N^0(\triangle). \tag{4.8}$$

We quote the estimate in [25, Theorem 3.4]:

$$\begin{aligned}\|\pi_N^{1,0}u - u\|_{1,\triangle} &\leq cN^{1-r}\left(\sum_{k_1+k_2+k_3=r} \big\|\partial_x^{k_1}\partial_y^{k_2}(\partial_y - \partial_x)^{k_3}u\big\|^2_{\omega_+^{k_1,k_2,k_3},\triangle}\right)^{1/2} \\ &\leq cN^{1-r}|u|_{r,\triangle},\end{aligned} \tag{4.9}$$

where

$$\omega_+^{k_1,k_2,k_3} = x^{\max(k_1+k_3-1,0)}y^{\max(k_2+k_3-1,0)}(1-x-y)^{\max(k_1+k_2-1,0)}.$$

Hence, the estimate (4.6) with $\mu = 1$ follows from (4.7) and (4.9).

To show (4.6) with $\mu = 0$, we use a duality argument as in [8], which we sketch below. Given $g \in L^2(\triangle)$, we consider the auxiliary problem: Find $u_g \in H_0^1(\triangle)$ such that

$$a(u_g, v) := (\nabla u_g, \nabla v)_\triangle = (g, v)_\triangle, \quad \forall\, v \in H_0^1(\triangle). \tag{4.10}$$

By a standard argument, we can show that this problem has a unique solution with the regularity $\|u_g\|_{2,\triangle} \leq c\|g\|_\triangle$.

Now, taking $v = u - \Pi_N^{1,0}u$ into (4.10), we find from (4.5)–(4.6) with $\mu = 1$ that

$$\begin{aligned}\big|(g, u - \Pi_N^{1,0}u)_\triangle\big| &= \big|a(u_g, u - \Pi_N^{1,0}u)\big| = \big|a(u_g - \Pi_N^{1,0}u_g, u - \Pi_N^{1,0}u)\big| \\ &\leq \big|u_g - \Pi_N^{1,0}u_g\big|_{1,\triangle}\big|u - \Pi_N^{1,0}u\big|_{1,\triangle} \\ &\leq cN^{-r}|u_g|_{2,\triangle}|u|_{r,\triangle} \leq cN^{-r}\|g\|_\triangle|u|_{r,\triangle}.\end{aligned}$$

Finally, we derive

$$\left\|u-\Pi_N^{1,0}u\right\|_{\triangle}=\sup_{0\neq g\in L^2(\triangle)}\frac{\left|(g,u-\Pi_N^{1,0}u)_{\triangle}\right|}{\|g\|_{\triangle}}\leq cN^{-r}|u|_{r,\triangle}.$$

This completes the proof. □

Remark 4.1 It is seen that benefited from the fact that $\mathcal{P}_N(\triangle)\subset Y_N(\triangle)$, we are able to obtain the optimal error estimates directly from the available polynomial approximation results on triangles. □

Remark 4.2 We stress that the estimate of (4.6)-type is also valid for the H^1-projection with partially homogeneous Dirichlet data. Here, we just consider the one to be used in Section 5, and outline the derivation below. Let

$$\Gamma=\big\{(x,y)\in\partial\triangle: xy=0\big\},\quad H^1_{\Gamma}(\triangle)=\big\{u\in H^1(\triangle): u|_{\Gamma}=0\big\}. \tag{4.11}$$

The orthogonal projection: $\Pi_N^{1,\Gamma}: H^1_{\Gamma}(\triangle)\to Y_N^{\Gamma}(\triangle)=Y_N(\triangle)\cap H^1_{\Gamma}(\triangle)$ is defined as in (4.5) with $\Pi_N^{1,\Gamma}$, $H^1_{\Gamma}(\triangle)$, $Y_N^{\Gamma}(\triangle)$ in place of $\Pi_N^{1,0}$, $H^1_0(\triangle)$, $Y_N^0(\triangle)$, respectively. We claim that for any $u\in H^1_{\Gamma}(\triangle)\cap H^r(\triangle)$ with $r\geq 1$, we have

$$\|\Pi_N^{1,\Gamma}u-u\|_{\mu,\triangle}\leq cN^{\mu-r}|u|_{r,\triangle},\quad \mu=0,1. \tag{4.12}$$

Clearly, this result with $r=\mu=1$ follows from the definition of $\Pi_N^{1,\Gamma}$ and the Poincaré inequality. Next, like the proof of Theorem 4.2, we look for an intermediate $u_N\in Y_N^{\Gamma}(\triangle)$, enjoying the approximation property:

$$\|\nabla(u_N-u)\|_{\triangle}\leq cN^{1-r}|u|_{r,\triangle},\quad r\geq 2. \tag{4.13}$$

The construction of u_N essentially follows the idea in [25], and makes use of the generalized Jacobi polynomials (cf. [16]). Define

$$J_0^{-1,-1}(\zeta)=1,\quad J_1^{-1,-1}(\zeta)=\zeta,\quad J_n^{-1,-1}(\zeta)=\frac{\zeta^2-1}{4}J_{n-2}^{1,1}(\zeta),\quad n\geq 2,$$

$$J_0^{\beta,-1}(\zeta)=1,\quad J_n^{\beta,-1}(\zeta)=\frac{n+\beta}{n}\frac{\zeta+1}{2}J_{n-1}^{\beta,1}(\zeta),\quad n\geq 1,\ \beta>-1,\ \zeta\in(-1,1).$$

Then

$$\mathcal{J}_{l_1,l_2}^{-1,-1,-1}(x,y)=(y+x)^{l_1}J_{l_1}^{-1,-1}\Big(\frac{y-x}{y+x}\Big)J_{l_2}^{2l_1-1,-1}(1-2x-2y),\quad l_1\geq 0,\ l_2\geq 0,$$

form a complete polynomial basis in $L^2(\triangle)$. In particular, $\{\mathcal{J}_{l_1,l_2}^{-1,-1,-1}\}_{l_1\geq 2,\,l_2\geq 0}$ forms a complete polynomial basis in $H^1_{\Gamma}(\triangle)$. For any $u\in H^1_{\Gamma}(\triangle)$, we write

$$u(x,y)=\sum_{l_1\geq 2,l_2\geq 0}\hat{u}_{l_1,l_2}\mathcal{J}_{l_1,l_2}^{-1,-1,-1}(x,y),$$

and define

$$u_N(x,y)=\sum_{\substack{l_1\geq 2,l_2\geq 0\\ l_1+l_2\leq N}}\hat{u}_{l_1,l_2}\mathcal{J}_{l_1,l_2}^{-1,-1,-1}(x,y)\in Y_N^{\Gamma}(\triangle).$$

Following the same lines as in the proof of Theorem 3.4 in [25], we can obtain

$$\begin{aligned}
\left\|\nabla(u-u_N)\right\|_{\triangle}^2 \le\ & cN^{-2}\left(\left\|\left(I_d-\pi_{N-2}^{0,0,1}\right)\partial_x\partial_y u\right\|_{\omega^{0,0,1},\triangle}^2\right.\\
&+\left\|\left(I_d-\pi_{N-2}^{1,0,0}\right)\partial_x\left(\partial_y-\partial_x\right)u\right\|_{\omega^{1,0,0},\triangle}^2\\
&\left.+\left\|\left(I_d-\pi_{N-2}^{0,1,0}\right)\partial_y\left(\partial_y-\partial_x\right)u\right\|_{\omega^{0,1,0},\triangle}^2\right)\\
\le\ & cN^{2-2r}\sum_{k_1+k_2+k_3=r-2}\left\|\partial_x^{k_1+1}\partial_y^{k_2+1}\left(\partial_y-\partial_x\right)^{k_3}u\right\|_{\omega^{k_1+k_3,k_2+k_3,k_1+k_2+1},\triangle}^2\\
&+cN^{2-2r}\sum_{k_1+k_2+k_3=r-2}\left\|\partial_x^{k_1}\partial_y^{k_2+1}\left(\partial_y-\partial_x\right)^{k_3+1}u\right\|_{\omega^{k_1+k_3,k_2+k_3+1,k_1+k_2},\triangle}^2\\
&+cN^{2-2r}\sum_{k_1+k_2+k_3=r-2}\left\|\partial_x^{k_1+1}\partial_y^{k_2}\left(\partial_y-\partial_x\right)^{k_3+1}u\right\|_{\omega^{k_1+k_3+1,k_2+k_3,k_1+k_2},\triangle}^2\\
\le\ & cN^{2-2r}|u|_{r,\triangle}^2,\quad r\ge 2,
\end{aligned}\tag{4.14}$$

where I_d is the identity operator, and $\pi_N^{\alpha_1,\alpha_2,\alpha_3}$ is the best $L^2_{\omega^{\alpha_1,\alpha_2,\alpha_3}}$-approximation in $\mathcal{P}_N(\triangle)$ as in [25]. Then by the definition of $\Pi_N^{1,\Gamma}$ and the Poincaré inequality, we have

$$\|\Pi_N^{1,\Gamma}u-u\|_{1,\triangle}\le c\|\nabla(u-u_N)\|_{\triangle}\le cN^{1-r}|u|_{r,\triangle},\quad r\ge 2.$$

Since the result with $r=1$ is shown, we obtain (4.12) for $\mu=0$ by using the duality argument as in the proof of Theorem 4.2. □

4.2 Estimation of interpolation error

Now, we estimate the error of interpolation by (3.28) on $\triangle$. The estimate of the one-dimensional LGL interpolation (cf. (3.26)) is useful for our analysis (see [33, Theorem 3.44]), that is, for any $v\in H^r(I)$ with $r\ge 1$, we have

$$\left\|I_N^{\zeta}v-v\right\|_{L^2(I)}\le cN^{-r}\left\|(1-\zeta^2)^{(r-1)/2}v^{(r)}\right\|_{L^2(I)}.\tag{4.15}$$

Theorem 4.3 *For any $u\in H^r(\triangle)$ with $r\ge 2$,*

$$\|\mathbb{I}_N u-u\|_{\triangle}\le cN^{-r}B_r(u),\tag{4.16}$$

where

$$B_r(u)=\begin{cases}|u|_{2,\triangle}+\|(\partial_y-\partial_x)^2u\|_{J^{-1},\triangle}+\|\nabla\cdot u\|_{J^{-1},\triangle}, & \text{if } r=2,\\ |u|_{r,\triangle}+|u|_{r-1,\triangle}, & \text{if } r\ge 3,\end{cases}\tag{4.17}$$

and J is the Jacobian as defined in (2.4).

Proof To this end, let I_d be the identity operator as before. Using (2.6), (3.28) and (4.15), we obtain

$$\begin{aligned}\big\| \mathbb{I}_N u - u\big\|_{\triangle} &\le c\big\| I_N^{\xi} I_N^{\eta}\tilde{u} - \tilde{u}\big\|_{\square}\\ &= c\big\|(I_N^{\xi} - I_d)(I_N^{\eta} - I_d)\tilde{u} + (I_N^{\xi} - I_d)\tilde{u} + (I_N^{\eta} - I_d)\tilde{u}\big\|_{\square}\\ &\le c\big(\big\|(I_N^{\xi} - I_d)(I_N^{\eta} - I_d)\tilde{u}\big\|_{\square} + \big\|(I_N^{\xi} - I_d)\tilde{u}\big\|_{\square} + \big\|(I_N^{\eta} - I_d)\tilde{u}\big\|_{\square}\big)\\ &\le cN^{-1}\big\|(I_N^{\eta} - I_d)\partial_{\xi}\tilde{u}\big\|_{\square} + c\big(\big\|(I_N^{\xi} - I_d)\tilde{u}\big\|_{\square} + \big\|(I_N^{\eta} - I_d)\tilde{u}\big\|_{\square}\big)\\ &\le cN^{-r}\big(\big\|(1-\eta^2)^{(r-2)/2}\partial_{\xi}\partial_{\eta}^{r-1}\tilde{u}\big\|_{\square} + \big\|(1-\xi^2)^{(r-1)/2}\partial_{\xi}^{r}\tilde{u}\big\|_{\square}\\ &\quad + \big\|(1-\eta^2)^{(r-1)/2}\partial_{\eta}^{r}\tilde{u}\big\|_{\square}\big).\end{aligned}$$

It remains to transform the variables (ξ, η) back to (x, y) and obtain tight upper bounds of the right-hand side using norms of u on $\triangle$. By (2.3),

$$\partial_{\xi}\tilde{u} = \frac{1-\eta}{4}\partial_y u - \frac{3-\eta}{8}(\partial_y - \partial_x)u = \frac{1-\eta}{4}\partial_x u - \frac{1+\eta}{8}(\partial_y - \partial_x)u, \tag{4.18}$$

$$\partial_{\eta}\tilde{u} = \frac{1-\xi}{4}\partial_x u + \frac{3-\xi}{8}(\partial_y - \partial_x)u = \frac{1-\xi}{4}\partial_y u + \frac{1+\xi}{8}(\partial_y - \partial_x)u. \tag{4.19}$$

Thus, we have

$$\partial_{\xi}^{r}\tilde{u} = \sum_{k=0}^{r}(-1)^k\binom{r}{k}\left(\frac{1+\eta}{8}\right)^k\left(\frac{1-\eta}{4}\right)^{r-k}\partial_x^{r-k}(\partial_y - \partial_x)^k u, \tag{4.20}$$

and

$$\begin{aligned}\big\|(1-\xi^2)^{(r-1)/2}\partial_{\xi}^{r}\tilde{u}\big\|_{\square}^2 &= \iint_{\square}|\partial_{\xi}^{r}\tilde{u}|^2(1-\xi^2)^{r-1}\mathrm{d}\xi\mathrm{d}\eta\\ &\le c\sum_{k=0}^{r}\iint_{\triangle}\big|\partial_x^{r-k}(\partial_y - \partial_x)^k u\big|^2\frac{Q(\xi,\eta;r,k)}{J}\,\mathrm{d}x\mathrm{d}y,\end{aligned}$$

where

$$Q(\xi,\eta;r,k) = \left(\frac{1+\eta}{8}\right)^{2k}\left(\frac{1-\eta}{4}\right)^{2r-2k}(1-\xi^2)^{r-1}.$$

One verifies readily from (2.1) that

$$\frac{1}{4}(1-\xi)(1-\eta) = 1 - x - y, \tag{4.21}$$

$$\frac{1}{4}(1+\xi)(1-\eta) + \frac{1}{8}(1+\xi)(1+\eta) = x, \tag{4.22}$$

$$\frac{1}{4}(1-\xi)(1+\eta) + \frac{1}{8}(1+\xi)(1+\eta) = y. \tag{4.23}$$

Therefore, by (4.21)–(4.23), we derive that for $2 \le r \le k-1$,

$$\begin{aligned} Q(\xi,\eta;r,k) &= \frac{1}{2^k}\Big[(1+\xi)^k\Big(\frac{1+\eta}{8}\Big)^k\Big]\Big[(1-\xi)^k\Big(\frac{1+\eta}{4}\Big)^k\Big] \\ &\quad\times\Big(\frac{(1+\xi)(1-\eta)}{4}\Big)^{r-k-1}\Big(\frac{(1-\xi)(1-\eta)}{4}\Big)^{r-k-1}\frac{(1-\eta)^2}{16} \\ &\le cx^k y^k x^{r-k-1}(1-x-y)^{r-k-1}J^2 \le c\varpi^{r-1,k,r-k-1}J, \end{aligned}$$

where we used the fact: $1-\eta \le 2-\xi-\eta = 16J$, and denoted by $\varpi^{\alpha,\beta,\gamma} = x^\alpha y^\beta(1-x-y)^\gamma$. Similarly, for $2 \le r = k$,

$$\begin{aligned} Q(\xi,\eta;r,k) &= \frac{1}{2^r}\Big(\frac{(1+\xi)(1+\eta)}{8}\Big)^{r-1}\Big(\frac{(1-\xi)(1+\eta)}{4}\Big)^{r-2}\Big(\frac{(1+\eta)}{4}\Big)^2(1-\xi) \\ &\le cx^{r-1}y^{r-2}J \le c\varpi^{r-1,r-2,0}J, \end{aligned}$$

where we used $1-\xi \le 2-\xi-\eta = 16J$. Consequently, we obtain for $r \ge 2$,

$$\begin{aligned} &\big\|(1-\xi^2)^{(r-1)/2}\partial_\xi^r\tilde{u}\big\|_\square \\ &\le c\left(\sum_{k=0}^{r-1}\big\|\partial_x^{r-k}(\partial_y-\partial_x)^k u\big\|^2_{\varpi^{r-1,k,r-k-1},\triangle} + \big\|(\partial_y-\partial_x)^r u\big\|^2_{\varpi^{r-1,r-2,0},\triangle}\right)^{\frac{1}{2}} \\ &\le c\big(|u|_{r-1,\triangle}+|u|_{r,\triangle}\big). \end{aligned} \tag{4.24}$$

By swapping $x \leftrightarrow y$ and $\xi \leftrightarrow \eta$, we get that for $r \ge 2$,

$$\big\|(1-\eta^2)^{(r-1)/2}\partial_\eta^r\tilde{u}\big\|_\square \le c\big(|u|_{r-1,\triangle}+|u|_{r,\triangle}\big). \tag{4.25}$$

We now turn to deal with the term $\big\|(1-\xi^2)^{(r-2)/2}\partial_\eta\partial_\xi^{r-1}\tilde{u}\big\|_\square$. By (4.19)–(4.20),

$$\begin{aligned} \partial_\eta\partial_\xi^{r-1}\tilde{u} &= \partial_\eta\left[\sum_{k=0}^{r-1}(-1)^k\binom{r-1}{k}\Big(\frac{1+\eta}{8}\Big)^k\Big(\frac{1-\eta}{4}\Big)^{r-k-1}\partial_x^{r-k-1}(\partial_y-\partial_x)^k u\right] \\ &= \sum_{k=0}^{r} W_1(\xi,\eta;r,k)\partial_x^{r-k}(\partial_y-\partial_x)^k u \\ &\quad+\sum_{k=0}^{r-1} W_2(\xi,\eta;r,k)\partial_x^{r-k-1}(\partial_y-\partial_x)^k u, \end{aligned} \tag{4.26}$$

where W_1 and W_2 are polynomials of ξ and η. Thus, we have

$$\begin{aligned} \big\|(1-\xi^2)^{(r-2)/2}\partial_\eta\partial_\xi^{r-1}\tilde{u}\big\|^2_\square &\le c\sum_{k=0}^{r}\iint_\triangle\Big|\partial_x^{r-k}(\partial_y-\partial_x)^k u\Big|^2\frac{(1-\xi^2)^{r-2}}{J}\,\mathrm{d}x\mathrm{d}y \\ &\quad+c\sum_{k=0}^{r-1}\iint_\triangle\Big|\partial_x^{r-k-1}(\partial_y-\partial_x)^k u\Big|^2\frac{(1-\xi^2)^{r-2}}{J}\,\mathrm{d}x\mathrm{d}y. \end{aligned}$$

This implies that for $r \geq 3$,

$$\left\|(1-\xi^2)^{(r-2)/2}\partial_\eta \partial_\xi^{r-1}\tilde{u}\right\|_{\square} \leq c\big(|u|_{r-1,\triangle} + |u|_{r,\triangle}\big). \tag{4.27}$$

For $r = 2$, we obtain from a direct calculation that

$$\|\partial_\xi \partial_\eta \tilde{u}\|_{\square} \leq |u|_{2,\triangle} + \frac{1}{256}\|(\partial_y - \partial_x)^2 u\|_{J^{-1},\triangle} + \frac{1}{64}\|\nabla \cdot u\|_{J^{-1},\triangle}. \tag{4.28}$$

A combination of (4.24)–(4.25) and (4.27)–(4.28) leads to the desired result. □

Remark 4.3 Like (4.24), we could obtain sharper estimates with semi-norms in the upper bound of (4.16) featured with the Jacobi-type weight functions $\varpi^{\alpha,\beta,\gamma}$.

Notice that for $r = 2$, the semi-norms are weighted with J^{-1}, as we cannot factor out $1-\xi$ or $1-\eta$ from W_1 and W_2 in (4.26) to eliminate J^{-1}. However, we point out that the value of $\iint_\triangle J^{-1}\mathrm{d}x\mathrm{d}y$ is finite. □

5 Numerical results and concluding remarks

In this section, we provide some numerical results to show the high accuracy of the proposed algorithm for model elliptic problems on $\triangle$. We also intend to compare it with the standard tensor-product spectral approximations on rectangles and polynomial approximation using the Duffy's transform to assess the performance of our approach.

5.1 The scheme and its convergence

Consider the elliptic equation:

$$-\Delta u + \gamma u = f, \quad \text{in } \triangle, \quad u|_{\Gamma_1} = 0, \quad \frac{\partial u}{\partial v}\Big|_{\Gamma_2} = g, \tag{5.1}$$

where the constant $\gamma \geq 0$, Γ_1 is the union of the edges $x = 0$ and $y = 0$ on $\triangle$, Γ_2 is the hypotenuse of $\triangle$, and v is the unit outer normal vector to Γ_2.

A weak formulation of (5.1) is to find $u \in H^1_{\Gamma_1}(\triangle) := \big\{u \in H^1(\triangle) : u|_{\Gamma_1} = 0\big\}$ such that

$$\mathcal{B}(u,v) := (\nabla u, \nabla v)_\triangle + \gamma(u,v)_\triangle = (f,v)_\triangle + \gamma\langle g, v\rangle_{\Gamma_2}, \quad \forall\, v \in H^1_{\Gamma_1}(\triangle), \tag{5.2}$$

where $\langle\cdot,\cdot\rangle_{\Gamma_2}$ is the inner product of $L^2(\Gamma_2)$. It follows from a standard argument that if $f \in L^2(\triangle)$ and $g \in L^2(\Gamma_2)$, the problem (5.2) admits a unique solution in $H^1_{\Gamma_1}(\triangle)$.

The spectral-Galerkin approximation of (5.2) is to find $u_N \in Y_N^{\Gamma_1}(\triangle) := Y_N(\triangle) \cap H^1_{\Gamma_1}(\triangle)$ such that for any $v_N \in Y_N^{\Gamma_1}(\triangle)$,

$$\mathcal{B}_N(u_N, v_N) := (\nabla u_N, \nabla v_N)_\triangle + \gamma(u_N, v_N)_\triangle = (\mathbb{I}_N f, v_N)_\triangle + \langle g, v_N\rangle_{N,\Gamma_2}, \tag{5.3}$$

where $\mathbb{I}_N$ is the interpolation operator as defined in (3.29), and the discrete inner product $\langle g, v_N\rangle_{N,\Gamma_2}$ can be defined on the quadrature rule:

$$\begin{aligned}\int_{\Gamma_2} g\,\mathrm{d}\gamma &= \frac{\sqrt{2}}{4}\left[\int_{-1}^{1}\tilde{g}(\xi,1)\mathrm{d}\xi+\int_{-1}^{1}\tilde{g}(1,\eta)\mathrm{d}\eta\right]\\ &\sim \frac{1}{2\sqrt{2}}\left[\sum_{j=0}^{N}\big(\tilde{g}(\zeta_j,1)+\tilde{g}(1,\zeta_j)\big)\omega_j\right],\end{aligned}\tag{5.4}$$

where $\{\zeta_j,\omega_j\}$ are the LGL interpolation nodes and weights as before. More precisely, we define

$$\langle g, v_N\rangle_{N,\Gamma_2}=\frac{1}{2\sqrt{2}}\sum_{j=0}^{N}\tilde{g}(\zeta_j,1)\tilde{v}_N(\zeta_j,1)\omega_j+\frac{1}{2\sqrt{2}}\sum_{j=0}^{N}\tilde{g}(1,\zeta_j)\tilde{v}_N(1,\zeta_j)\omega_j,\tag{5.5}$$

where $\tilde{g}=g\circ T$ and $\tilde{v}_N=v_N\circ T$.

Remark 5.1 Here, we purposely impose the Neumann boundary condition on the hypotenuse of $\triangle$, so that the basis functions associated with this "singular" edge are involved in the computation.

We reiterate that a distinctive difference with the scheme in [27, (25)] lies in that the consistency condition (2.9) is not needed to be built in the approximation space, which significantly facilitates the implementation. Note that the approaches based on the Duffy's transform also need to modify the basis functions to meet the corresponding consistency condition (see e.g., [5, 34]). □

Apart from the result (4.12) in Remark 4.2, another ingredient for the analysis is to estimate the error between the continuous and discrete inner products on Γ_2. Given $g\in H^t(\Gamma_2)$, using [33, Lemma 4.8] leads to

$$\begin{aligned}\big|\langle g, v_N\rangle_{N,\Gamma_2}-\langle g, v_N\rangle_{\Gamma_2}\big| \le cN^{-t}\Big(&\big\|(1-\xi^2)^{(t-1)/2}\partial_\xi^t\tilde{g}(\cdot,1)\big\|_{L^2(I)}\|\tilde{v}_N(\cdot,1)\|_{L^2(I)}\\ &+\big\|(1-\eta^2)^{(t-1)/2}\partial_\eta^t\tilde{g}(1,\cdot)\big\|_{L^2(I)}\|\tilde{v}_N(1,\cdot)\|_{L^2(I)}\Big).\end{aligned}$$

Then we obtain from (4.18)–(4.19) and a derivation similar to the proof of Theorem 4.3 the following estimate:

$$\begin{aligned}\big|\langle g, v_N\rangle_{N,\Gamma_2}-\langle g, v_N\rangle_{\Gamma_2}\big| &\le cN^{-t}\|(xy)^{(t-1)/2}(\partial_y-\partial_x)^t g\|_{\Gamma_2}\|v_N\|_{\Gamma_2}\\ &\le cN^{-t}|g|_{t,\Gamma_2}\|v_N\|_{\Gamma_2},\quad t\ge 1.\end{aligned}\tag{5.6}$$

With the above preparations, we can prove the convergence of the scheme (5.3) by using (4.12), Theorem 4.3, the estimate (5.6) and a standard argument for error estimate of spectral approximation of elliptic problems.

Theorem 5.1 *Let u and u_N be the solutions of (5.2) and (5.3), respectively. If $u \in H^1_{\Gamma_1}(\triangle) \cap H^r(\triangle)$, $f \in H^s(\triangle)$ and $g \in H^t(\Gamma_2)$ with $r \geq 1, s \geq 2$ and $t \geq 1$, then we have*

$$\|u - u_N\|_{\mu,\triangle} \leq c\big(N^{\mu-r}|u|_{r,\triangle} + N^{-s}B_s(f) + N^{-t}|g|_{t,\Gamma_2}\big),$$

where $\mu = 0, 1$, $B_s(f)$ is defined in (4.17), and c is a positive constant independent of N, u, f and g.

5.2 Numerical results

5.2.1 Example 1

We first intend to show the typical spectral accuracy of the proposed method, so we particularly test it on (5.1) with $\gamma = 1$ and the exact solution:

$$u(x, y) = e^{x+y-1} \sin\big(3xy\big(y - \sqrt{3}x/2 + \sqrt{3}/4\big)\big), \quad \forall\, (x, y) \in \triangle. \tag{5.7}$$

For comparison, we also consider the standard tensor polynomial approximation of (5.1) on a square $S = (0, 1/\sqrt{2})^2$ (note: it has the same area as $\triangle$) under a similar setting, i.e., Neumann data on two edges $x = 1/\sqrt{2}$ and $y = 1/\sqrt{2}$, and homogeneous Dirichlet data on the other two edges. We take the exact solution:

$$u(x, y) = \exp\left(-\left(\frac{1}{\sqrt{2}} - x\right)\left(\frac{1}{\sqrt{2}} - y\right)\right) \sin\big(3xy\big(y - \sqrt{3}x/2 + \sqrt{3}/4\big)\big), \quad \forall (x, y) \in S. \tag{5.8}$$

In Fig. 5, we plot the numerical errors of two methods, from which we observe that they share a very similar convergence behavior and the errors decay like $O(e^{-cN})$. For a fixed N, the accuracy of approximation on S seems to be slightly better than expected. Indeed, the accuracy is comparable to the existing means in [22, 27, 34].

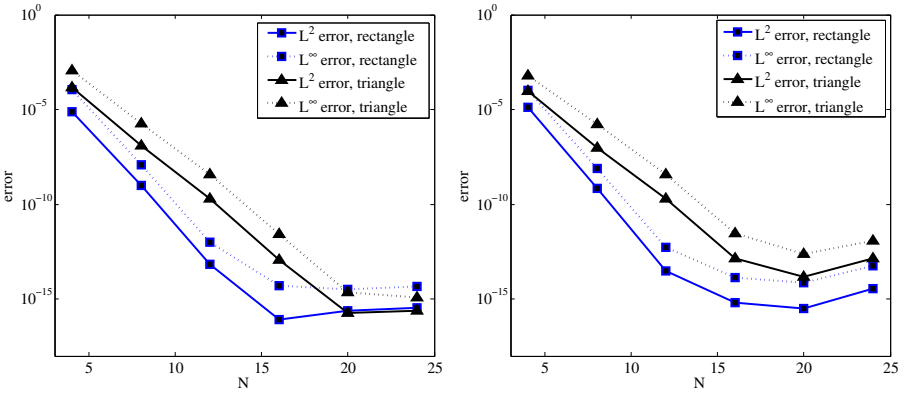

Fig. 5 Numerical errors of (5.3) vs. tensorial polynomial approximation on the *square* S. *Left* L^2- and L^∞-errors using modal basis, (3.4) on $\square$ and (3.5) on $\triangle$. *Right* L^2- and L^∞-errors using nodal basis, $\{h_k h_l\}_{k,l=0}^N$ on $\square$ and (3.31) on $\triangle$

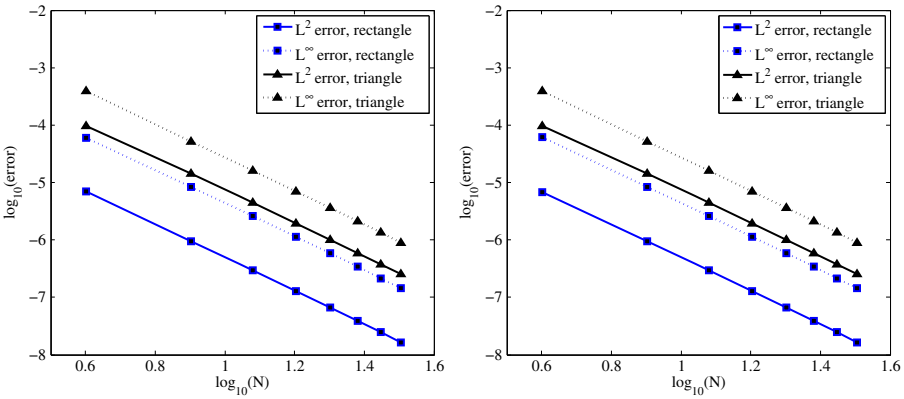

Fig. 6 Numerical errors of (5.3) vs. tensorial polynomial approximation on the *square* S with solutions having finite regularity. *Left* L^2- and L^∞-errors using modal basis, (3.4) on $\square$ and (3.5) on $\triangle$. *Right* L^2- and L^∞-errors using nodal basis, $\{h_k h_l\}_{k,l=0}^N$ on $\square$ and (3.31) on $\triangle$

5.2.2 Example 2

In the second test, we choose the exact solution of (5.1) with finite regularity (with $\gamma = 1$):

$$u(x, y) = (1 - x - y)^{\frac{5}{2}}(e^{xy} - 1), \quad \forall\, (x, y) \in \triangle, \tag{5.9}$$

which belongs to $H^{3-\epsilon}(\triangle)$ (for small $\epsilon > 0$). The counterpart on the square S takes the form:

$$u(x, y) = \left(\frac{1}{\sqrt{2}} - x\right)^{\frac{5}{2}} \left(\frac{1}{\sqrt{2}} - y\right)^{\frac{5}{2}} (e^{xy} - 1), \quad \forall\, (x, y) \in S. \tag{5.10}$$

We depict in Fig. 6 the numerical errors of two approaches in log-log scale, where the slopes of the lines are all roughly -3 as predicted by the theoretical results (cf. Theorem 5.1).

5.2.3 Comparison with the nodal approach in [27]

We compare our new approach with the method in [27], where the explicit consistency condition (2.9) was built in the approximation space. We test the same problem with the same exact solution. One can see from Table 2 that both approaches enjoy a similar convergence behavior. We reiterate that the new method does not require

Table 2 Comparison between the approach in [27] and the new method

N	Approach in [27]		Approach in this paper	
	L^2-error	L^∞-error	L^2-error	L^∞-error
15	$2.866E{-}06$	$1.018E{-}05$	$2.349E{-}06$	$8.281E{-}06$
30	$3.410E{-}07$	$1.203E{-}06$	$3.087E{-}07$	$1.091E{-}06$
45	$9.940E{-}08$	$3.513E{-}07$	$9.299E{-}08$	$3.283E{-}07$

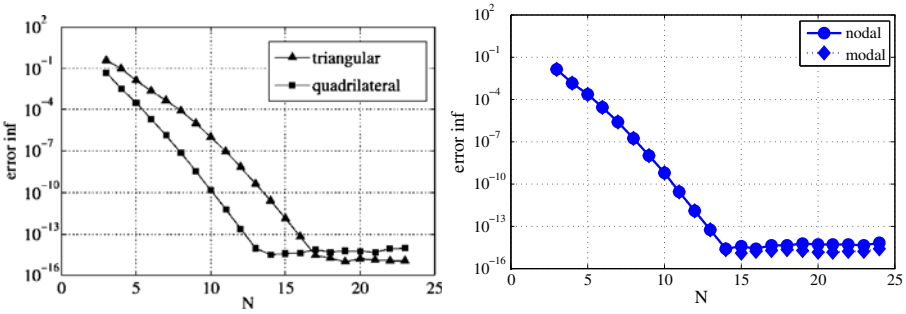

Fig. 7 L^∞-errors against N. *Left* From [3, Fig. 2.17], where tensorial quadrilateral approach on *rectangle* and Dubiner basis on *triangle* are used. *Right* Approach in this paper, where the modal basis and nodal basis are given in (3.5) and (3.31), respectively

to modify the basis function, so with a pre-computation of the stiffness matrix, the triangular element can be treated as efficiently as the quadrilateral element.

5.2.4 Comparison with the Dubiner basis

Finally, we test our approach on an existing example (see [3, Page 107]), where the spectral-Galerkin method based on the Dubiner polynomial basis (note: about $N^2/2$ degrees of freedom), is used. We adopt the same setting and solve the Poisson equation on the triangle $\{(x, y) : x, y \geq -1, x + y \leq 0\}$ with homogeneous Dirichlet boundary condition and exact solution: $(1 + x)(1 + y)(x + y) \exp(-(x + y))$.

We snapshot the figure in [3, Figure 2.17], and put it in Fig. 7 (left) for reference. Our result is depicted in Fig. 7 (right). Observe that by using N^2 degrees of freedom, our approach produces slightly better accuracy, and the decay of the errors follows more closely to the tensorial quadrilateral case.

5.3 Concluding remarks

We initiated in this paper a new TSEM through presenting the detailed implementation and analysis on a triangle. We demonstrated that the use of the rectangle–triangle mapping in [27] led to much favorable grid distributions, when compared with the commonly-used Duffy's transform. More importantly, we showed the induced singularity could be fully removed. It is anticipated that with this initiative, we can develop an efficient TSEM on unstructured meshes built on a suitable discontinuous Galerkin formulation. This will be discussed in a forthcoming work.

References

1. Adams, R.A.: Sobolev Spaces. Acadmic Press, New York (1975)
2. Boyd, J.P., Yu, F.: Comparing seven spectral methods for interpolation and for solving the Poisson equation in a disk: Zernike polynomials, Logan–Shepp ridge polynomials, Chebyshev–Fourier series, cylindrical Robert functions, Bessel–Fourier expansions, square-to-disk conformal mapping and radial basis functions. J. Comput. Phys. **230**(4), 1408–1438 (2011)

3. Canuto, C., Hussaini, M.Y., Quarteroni, A., Zang, T.A.: Spectral Methods: Fundamentals in Single Domains. Scientific Computation. Springer-Verlag, Berlin (2006)
4. Canuto, C., Hussaini, M.Y., Quarteroni, A., Zang, T.A.: Spectral Methods: Evolution to Complex Geometries and Applications to Fluid Dynamics. Scientific Computation. Springer, Berlin (2007)
5. Chen, L., Shen, J., Xu, C.: A triangular spectral method for the Stokes equations. Numer. Math.: Theory Methods Appl. **4**, 158–179 (2011)
6. Chen, Q., Babuška, I.M.: Approximate optimal points for polynomial interpolation of real functions in an interval and in a triangle. Comput. Methods Appl. Math. Eng. **128**(2), 405–417 (1995)
7. Chernov, A.: Optimal convergence estimates for the trace of the polynomial L^2-projection operator on a simplex. Math. Comput. **81**(278), 765–787 (2011)
8. Ciarlet, P.G.: The Finite Element Method for Elliptic Problems. North Holland, Amsterdam, The Netherlands (1978)
9. Cockburn, B., Gopalakrishnan, J., Lazarov, R.: Unified hybridization of discontinuous Galerkin, mixed, and continuous Galerkin methods for second order elliptic problems. SIAM J. Numer. Anal. **47**(2), 1319–1365 (2009)
10. Deville, M.O., Fischer, P.F., Mund, E.H.: High-Order Methods for Incompressible Fluid Flow. Cambridge Monographs on Applied and Computational Mathematics, vol. 9. Cambridge University Press, Cambridge (2002)
11. Dubiner, M.: Spectral methods on triangles and other domains. J. Sci. Comput. **6**(4), 345–390 (1991)
12. Duffy, M.G.: Quadrature over a pyramid or cube of integrands with a singularity at a vertex. SIAM J. Numer. Anal. **19**(6), 1260–1262 (1982)
13. Gautschi, W.: Gauss quadrature routines for two classes of logarithmic weight functions. Numer. Algorithms **55**(2–3), 265–277 (2010)
14. Gordon, W.J., Hall, C.A.: Construction of curvilinear co-ordinate systems and applications to mesh generation. Int. J. Numer. Methods Eng. **7**, 461–477 (1973)
15. Gradshteyn, I.S., Ryzhik, I.M.: Table of Integrals, Series and Products, 7th Edn. Academic Press, New York (2007)
16. Guo, B.Y., Shen, J., Wang, L.: Optimal spectral-Galerkin methods using generalized Jacobi polynomials. J. Sci. Comput **27**(1–3), 305–322 (2006)
17. Guo, B.Y., Wang, L.: Error analysis of spectral method on a triangle. Adv. Comput. Math. **26**(4), 473–496 (2007)
18. Heinrichs, W.: Spectral collocation schemes on the unit disc. J. Comput. Phys. **199**, 55–86 (2004)
19. Helenbrook, B.T.: On the existence of explicit *hp*-finite element methods using Gauss–Lobatto integration on the triangle. SIAM J. Numer. Anal. **47**(2), 1304–1318 (2009)
20. Hesthaven, J.S.: From electrostatics to almost optimal nodal sets for polynomial interpolation in a simplex. SIAM J. Numer. Anal. **35**(2), 655–676 (1998)
21. Hylleraas, E.A.: Linearization of products of Jacobi polynomials. Math. Scand. **10**, 189–200 (1962)
22. Karniadakis, G.E., Sherwin, S.J.: Spectral/*hp* Element Methods for Computational Fluid Dynamics. Numerical Mathematics and Scientific Computation, 2nd Edn. Oxford University Press, New York (2005)
23. Kirby, R.M., Sherwin, S.J., Cockburn, B.: To CG or to HDG: a comparative study. J. Sci. Comput. **51**(1), 183–212 (2012)
24. Koornwinder, T.: Two-Variable Analogues of the Classical Orthogonal Polynomials. In: Theory and Application of Special Functions (Proc. Advanced Sem., Math. Res. Center, Univ. Wisconsin, Madison, Wis., 1975) pp. 435–495. Math. Res. Center, Univ. Wisconsin, Publ. No, p. 35. Academic Press, New York (1975)
25. Li, H., Shen, J.: Optimal error estimates in Jacobi-weighted Sobolev spaces for polynomial approximations on the triangle. Math. Comput. **79**(271), 1621–1646 (2010)
26. Li, H., Wang, L.: A spectral method on tetrahedra using rational basis functions. Int. J. Numer. Anal. Model. **7**(2), 330–355 (2010)
27. Li, Y., Wang, L., Li, H., Ma, H.: A New Spectral Method on Triangles. In: Spectral and High Order Methods for Partial Differential Equations: Selected papers from the ICOSAHOM '09 conference, June 22–26, Trondheim, Norway. Lecture Notes in Computational Sciences and Engineering, Vol. 76, pp. 237–246. Springer, New York (2011)
28. Nguyen, N.C., Peraire, J., Cockburn, B.: Hybridizable Discontinuous Galerkin Methods. In: Spectral and High Order Methods for Partial Differential Equations: Selected Papers from the ICOSAHOM '09 Conference, June 22–26, Trondheim, Norway. Lecture Notes in Computational Sciences and Engineering, Vol. 76, pp. 63–84. Springer, New York (2011)

29. Pasquetti, R., Rapetti, F.: Spectral element methods on unstructured meshes: comparisons and recent advances. J. Sci. Comput. **27**(1–3), 377–387 (2006)
30. Pasquetti, R., Rapetti, F.: Spectral element methods on unstructured meshes: which interpolation points? Numer. Algorithms **55**(2–3), 349–366 (2010)
31. Patera, A.T.: A spectral element method for fluid dynamics: laminar flow in a channel expansion. J. Comput. Phys. **54**(3), 468–488 (1984)
32. Schwab, C.: p- and hp-Finite Element Methods: Theory and Applications in Solid and Fluid Mechanics. Numerical Mathematics and Scientific Computation. Oxford Science, Oxford, UK (1998)
33. Shen, J., Tang, T., Wang, L.: Spectral Methods: Algorithms, Analysis and Applications. Springer Series in Computational Mathematics, Vol. 41. Springer-Verlag, Berlin Heidelberg (2011)
34. Shen, J., Wang, L., Li, H.: A triangular spectral element method using fully tensorial rational basis functions. SIAM J. Numer. Anal. **47**(3), 1619–1650 (2009)
35. Szegö, G.: Orthogonal Polynomials, 4th Edn, Vol. 23. AMS Coll. Publ., Providence, RI (1975)
36. Taylor, M.A., Wingate, B.A., Vincent, R.E.: An algorithm for computing Fekete points in the triangle. SIAM J. Numer. Anal. **38**(5), 1707–1720 (2000)
37. Weber, H.: Lehrbuch der Algebra. Erster Band, Braunschweig (1912)
38. Xie, Z., Wang, L., Zhao, X.: On exponential convergence of Gegenbauer interpolation and spectral differentiation. Math. Comput., electronically published on 21 August 2012
39. Xu, Y.: Common Zeros of Polynomials in Several Variables and Higher Dimensional Quadrature. Chapman & Hall/CRC, London, UK (1994)
40. Xu, Y.: On Gauss–Lobatto integration on the triangle. SIAM J. Numer. Anal. **49**(2), 541–548 (2011)